Bulletin of the Seismological Society of America, Vol. 88, No. 1, pp. 183–205, February 1998

Estimates of Regional and Local Strong Motions during the Great 1923 Kanto, Japan, Earthquake (*Ms* 8.2). Part 1: Source Estimation of a Calibration Event and Modeling of Wave Propagation Paths

by Toshiaki Sato, Donald V. Helmberger, Paul G. Somerville, Robert W. Graves, and Chandan K. Saikia

Abstract This article is the first of a pair of articles that estimate regional and local strong motions from the 1923 Kanto, Japan, earthquake. This *Ms* 8.2 earthquake caused the most devastating damage in the metropolitan area in Tokyo history. In this article, we first calibrate wave propagation path effects with a moderate-sized modern event. This event, the Odawara earthquake of 5 August 1990 (*M* 5.1), is the first earthquake larger than *M* 5 in the last 60 years near the hypocenter of the 1923 Kanto earthquake. We estimate the source parameters based on a grid-search technique using body-waveform data bandpass filtered from 1 to 10 sec at four local stations, because accurate source parameters are critical for calibrating the propagation effects. We find that the Odawara earthquake had a depth of 15.3 km, a dip of 35°, a rake of 40°, a strike of 215°, a seismic moment of 3.3×10^{23} dyne-cm, a source duration of 0.65 sec, and a stress drop of 170 bars.

Next, we investigate the effects of the propagation paths to the local and regional stations where seismograms of the 1923 Kanto earthquake were recorded, by comparing recorded waveforms with synthetic seismograms built with the calibration event. Path-specific flat-layered velocity models are estimated along travel paths from the event to stations Hongo (epicentral distance $R = 82$ km) in Tokyo, Gifu ($R = 213$ km), and Sendai ($R = 374$ km) using forward modeling. In constructing the velocity model for the Gifu station, we use STS-1 broadband seismograms recorded at the nearby Inuyama station. Consequently, at periods greater than 3 sec, the velocity models for stations Hongo and Gifu can successfully reproduce both body waves and direct surface waves, and the velocity model for Sendai station can explain the predominant direct surface waves. In the companion article (Sato *et al.*, 1998), these velocity models are used to examine the adequacy of the variable-slip rupture models of the 1923 Kanto earthquake (Wald and Somerville, 1995; Takeo and Kanamori, 1992) to explain recorded seismograms and also to simulate strong motions from that event.

Introduction

The great 1923 Kanto earthquake (*Ms* 8.2) of 1 September 1923, which struck Tokyo and surrounding areas, was one of the most devastating earthquakes in Japanese history, and for this reason, the effects of this earthquake have been widely studied in earthquake-resistant design and emergency preparedness in Tokyo and other parts of Japan. Although several studies of this earthquake have been done, we conduct a much more systematic analysis of the recorded regional and local ground motions.

During the 1923 Kanto earthquake, near-fault strong ground motions were recorded by low-gain displacement seismographs: the Ewing seismoscope and the Imamura seismograph at Hongo (HNG) station in Tokyo, which is located at about 60 km northeast of the epicenter. Unfortunately, all of the seismograms were incomplete because the large displacements exceeded the recording range of the seismographs. Since the Imamura seismogram reconstructed by Yokota *et al.* (1989) differed significantly from the Ewing

seismogram restored by Nasu (1971a,b), Morioka (1980), and Morioka and Yamada (1986), as discussed in Takeo and Kanamori (1992), it is difficult to understand this earthquake using only the Ewing and Imamura seismograms at station HNG.

Recent developments in data acquisition and analysis have significantly enhanced our ability to understand this earthquake. First, seismograms recorded at several regional stations were found, and some of them have been digitized (Kudo, 1981; Kataoka and Sato, 1994; Kataoka *et al.,* 1995; Takemura, 1994; Takemura and Hamada, 1994, Takemura and Nozawa, 1994; Takemura *et al.,* 1994, 1995). The locations of the stations Sendai (SND), Hongo (HNG), and Gifu (GIF) at which we digitized seismograms are shown in Figure 1a. Processing of these seismograms recorded more than 70 years ago presented many challenges, such as the low quality of the data and uncertainty in instrument responses (Kataoka *et al.,* 1995; Takemura and Hamada, 1994; Takemura *et al.,* 1995). However, despite their limitations, these seismograms are valuable for a more complete understanding of both the source process and the strength of the strong motions from the 1923 Kanto earthquake, since some of the regional seismograms were not clipped.

The second important development is the derivation of a variable-slip rupture model from the joint inversion of geodetic and teleseismic body-waveform data by Wald and Somerville (1995). The periods for which the recorded ground motions can be reliably reproduced using the previous uniform slip models (Kanamori, 1971, 1974; Ando, 1971, 1974; Matsu'ura *et al.,* 1980) were limited to longer than several tens of seconds. In contrast, we expect the variable-slip rupture model derived by Wald and Somerville (1995) to reproduce recorded waveforms at periods as short as several seconds. If we can estimate the effects of wave propagation paths from the source region of the 1923 Kanto earthquake to regional and local sites where the seismograms were recorded, we will be able not only to examine the validity of the variable-slip rupture model derived by Wald and Somerville (1995) but also to estimate strong motions in the Tokyo metropolitan at periods of engineering significance.

In calibrating wave propagation paths from a historical earthquake, recordings from smaller or comparable-sized modern earthquakes occurring in the vicinity of the historical event can be used as calibration events (e.g., Helmberger *et al.,* 1992a; Wald *et al.,* 1993). The seismicity in the source region of the 1923 Kanto earthquake has been low for a long time, and only one earthquake of magnitude greater than 5.0 has occurred for the last 60 years in the region where large slip occurred during the 1923 Kanto earthquake (Wald and Somerville, 1995), although there has been recent activity in the Izu Peninsula, which is located southwest of the epicenter of the 1923 Kanto earthquake as determined by Kanamori and Miyamura (1970) and Hamada (1987). The earthquake, with M_{JMA} 5.1, occurred on 5 August 1990 at a depth of about 15 km beneath the Odawara area. The 1990 hypocenter is in the vicinity of the hypocenter of the 1923 Kanto earthquake and is also close to one of the two major asperities of the 1923 Kanto earthquake as determined by Wald and Somerville (1995) and shown in Figure 1b. Ishida and Kikuchi (1992) investigated the source process of the 1990 Odawara earthquake in detail and concluded that this earthquake is a possible foreshock of a future large earthquake in the region. In terms of location, size, and characteristics as a calibration event for investigating propagation path effects, this event seems to be more suitable than the Izu earthquakes. However, recently Pitarka *et al.* (1994) pointed out that the source model derived by Ishida and Kikuchi (1992) is not compatible with near-source strong-motion data. Therefore, to use this event as a calibration event, we need to re-evaluate the source model of this event.

The objectives of this article are twofold: (1) to develop a well-constrained source model of the 1990 Odawara earthquake, and (2) to use the recordings of this earthquake to calibrate flat-layered velocity models and to examine the adequacy of these velocity models for reproducing the effects of wave propagation paths between the source region of the 1923 Kanto earthquake and the regional stations Gifu (GIF) and Sendai (SND), and the local station Hongo (HNG) that recorded the 1923 Kanto earthquake. To accomplish the first objective, we use the grid-search technique using body-waveform data (Zhao and Helmberger, 1994). The synthetic seismograms are calculated by the frequency-wavenumber integration method (*f-k* method) (Saikia, 1994). The second objective is accomplished using a forward-modeling procedure based on the comparison between recorded waveform data and synthetic seismograms calculated by the *f-k* method and/or generalized ray theory (GRT) (Helmberger, 1983).

In the companion article (Sato *et al.,* 1998), the flat-layered velocity models derived in this study are used to examine the adequacy of the variable-slip rupture models of the 1923 Kanto earthquake (Wald and Somerville, 1995; Takeo and Kanamori, 1992) and to simulate the seismograms obtained at stations GIF, SND, and HNG from that earthquake.

Source Model of the 1990 Odawara Earthquake and Waveform Modeling at Local Stations

The source models of the 1990 Odawara earthquake derived from previous studies have some discrepancies in source location, mechanism, and seismic moment as indicated in Table 1 and Figure 1b. The National Research Institute for Earth Science and Disaster Prevention (NIED, 1990) determined the strike-slip mechanism shown in Figure 2a using the *P*-wave first motions from the NIED seismic network. Ishida and Kikuchi (1992) re-examined the source model using both short-period *P*-wave seismograms from the NIED seismic network and broadband waveform data recorded at two local stations, and they found that at some stations a strong phase with the opposite polarity was recorded a few tenths of a second after the *P*-wave onset. They attributed the polarity change to the difference between the

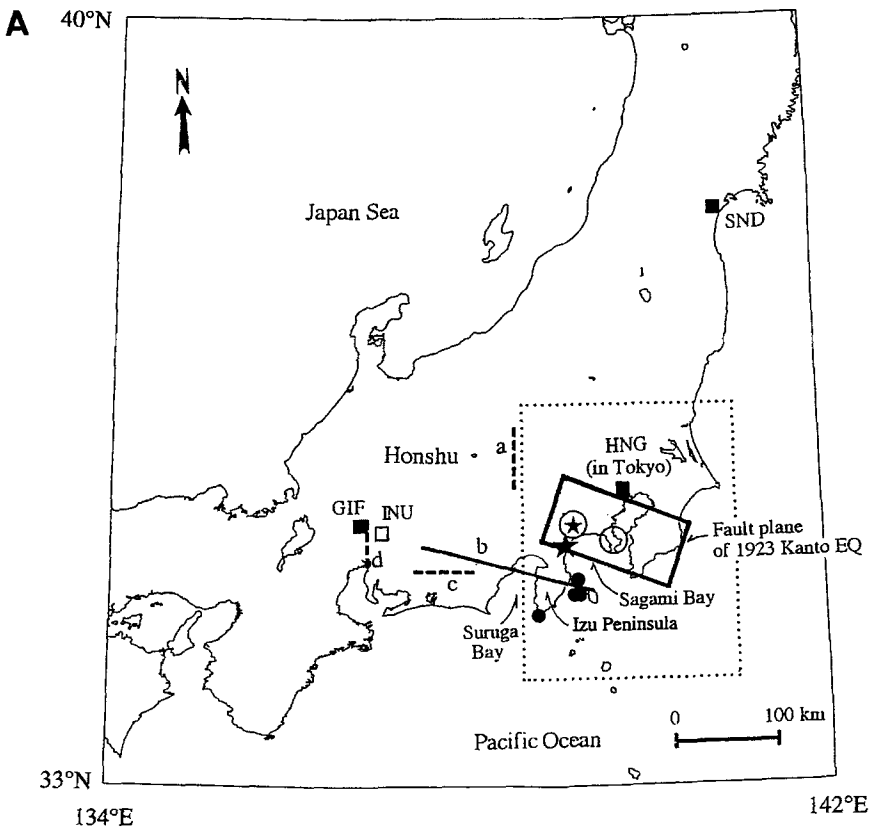

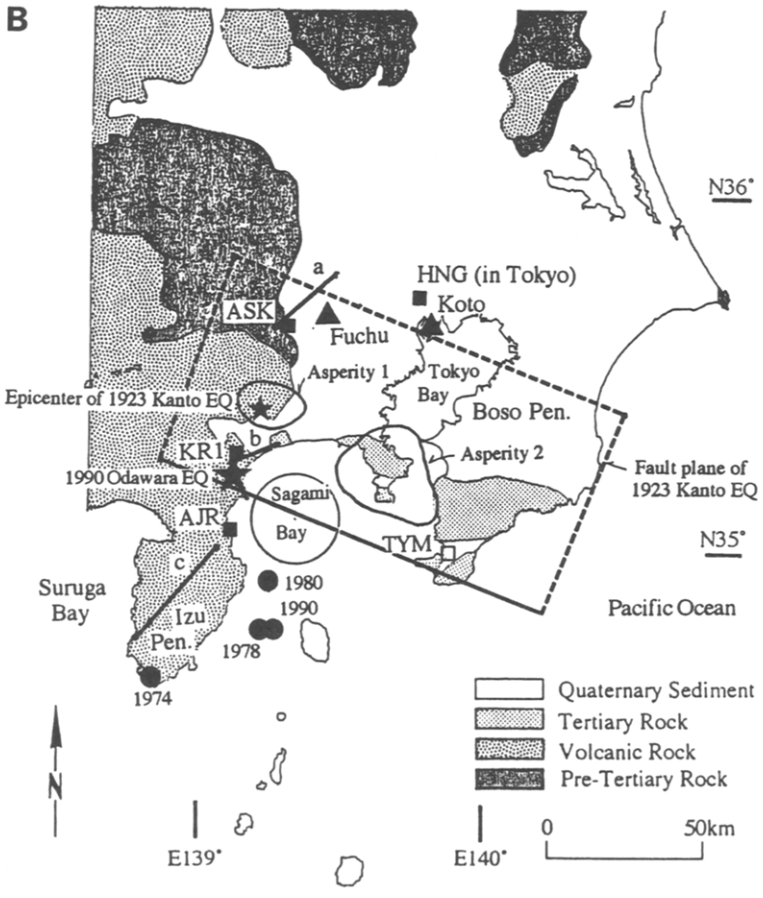

Figure 1. (a) Location map showing earthquakes and stations used in calibration of the travel paths in this study. The area surrounded by solid lines indicates the surface projection of the fault geometry of the 1923 Kanto earthquake (*Ms* 8.2). A small solid star denotes the epicenter of the 1923 Kanto earthquake estimated by Kanamori and Miyamura (1970). Open circles represent locations of asperities estimated by Wald and Somerville (1995). A large solid star denotes the epicenter of the 1990 Odawara earthquake (M_{JMA}5.1) used as the calibration event for the travel paths. Solid circles represent Izu earthquakes of magnitude greater than 6.5 in the past 40 years. Solid squares indicate stations Sendai (SND), Hongo (HNG), and Gifu (GIF) at which seismograms from both the 1923 Kanto earthquake and the 1990 Odawara earthquake were recorded by conventional seismographs. An open square indicates Inuyama (INU) station at which STS-1 broadband data from the 1990 Odawara earthquake were recorded. A solid line labeled b shows the seismic refraction survey conducted by Ikami (1978). Dashed lines labeled a, c, and d represent the lines of the shallow seismic refraction surveys conducted by Sasatani *et al.* (1990), Matsu'ura (1991), and Masaki and Iida (1981, 1982). The area surrounded by dotted lines is enlarged in Figure 1b, which shows the locations of stations AJR, ASK, HNG, and KR1 (solid squares) used in estimating the 1990 Odawara earthquake. Geologic conditions in the southern Kanto district are also shown. Solid lines a, b, and c are the lines of the seismic refraction surveys (Yoshii *et al.*, 1985; Yamanaka *et al.*, 1993; JESG, 1992) used for constructing the shallow crustal structure models for stations AJR, ASK, and KR1. Solid triangles denote the deep borehole sites at Koto (Suzuki, 1993, 1995) and Fuchu (Yamamizu *et al.*, 1981; Asano *et al.*, 1993) used in constructing shallow crustal structure models for stations HNG and ASK. The area surrounded by solid and dashed lines indicates the surface projection of the fault geometry of the 1923 Kanto earthquake (*Ms* 8.2); the solid line indicates the top edge of the fault plane. The first and second asperities correspond to the portions with slip greater than 4 m (Wald and Somerville, 1995). The 1974 Izu-Hanto-Oki earthquake (M_{JMA} 6.9) and the 1980 Izu-Hanto-Toho-Oki earthquake (M_{JMA}6.7) were used as calibration events in modeling the propagation path to station GIF by Nozawa *et al.* (1996).

Table 1
Source Models of the 1990 Odawara Earthquake

Model	Epicenter Lat. (°N)	Epicenter Long. (°E)	Depth (km)	Origin time (GT)	Dip (°)	Rake (°)	Strike (°)	M_0 ($\times 10^{23}$ dyne-cm)	Source-Time Function (sec)
NIED	35.212	139.110	15.3	1990/8/5 7:13:01.69	52	19	222	6.7*	bell shape (0.5)*
IK92	35.210	139.103	17.2	1990/8/5 7:13:01.63	50	70	210	3.5	triangle (0.3, 0.1)
JMA	35.207	139.095	13.7	1990/8/5 7:13:02.10	39	30	219	7.1†	—
HRV	34.950	138.840	15.0	1990/8/5 7:13:04.00	23	68	220	5.9	—
SATO	35.210‡	139.103‡	15.3	—	35	40	215	3.3	trapezoid (0.3, 0.2, 0.15)

*Pitarka *et al.* (1994).
†This value is estimated from $M_{JMA} = 5.1$ based on $\log M_0 = 1.5M_{JMA} + 16.2$ (Sato, 1979).
‡The epicenter is assumed to be the same as that of the IK92 solution (Ishida and Kikuchi, 1992).

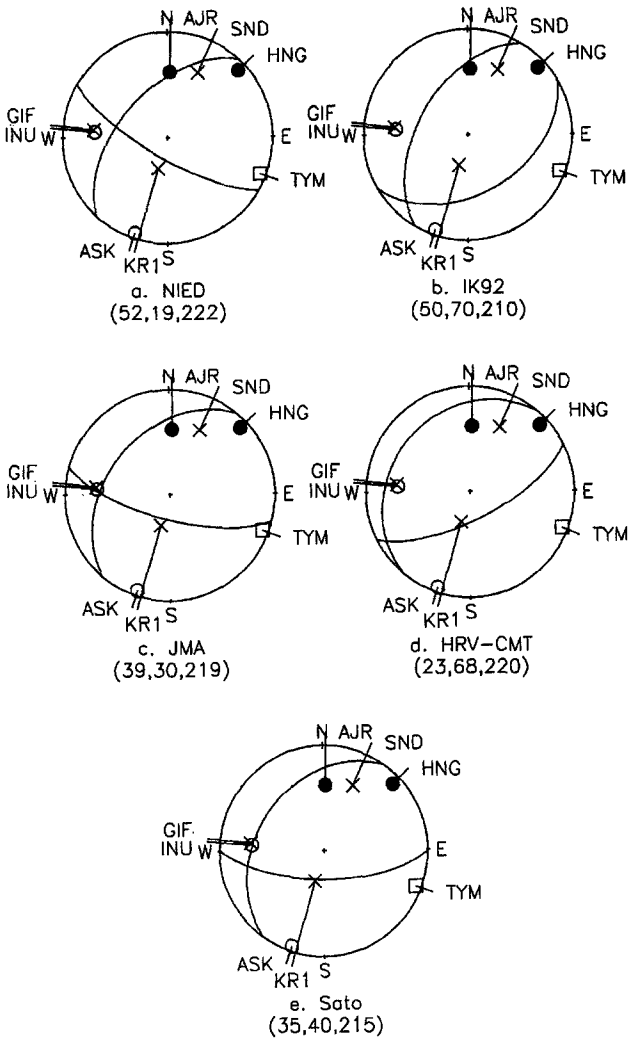

Figure 2. Comparison between the focal mechanisms of the 1990 Odawara earthquake derived by the National Research Institute for Earth Science and Disaster Prevention [(a) NIED solution], Ishida and Kikuchi (1992) [(b) IK92 solution], Japan Meteorological Agency [(c) JMA solution], Harvard University [(d) HRV CMT solution], and the best-fit solution in this study [(e) Sato solution], respectively. All fault-plane solutions are lower hemispheric projections.

focal mechanism of the initial rupture and that of the main rupture, and they estimated a dip-slip reverse faulting mechanism for the main rupture referred to as IK92 shown in Figure 2b. The Japan Meteorological Agency (1990), using *P*-wave first-motion data from the JMA seismic network, obtained a fault-plane solution showing strike-slip faulting referred to as JMA shown in Figure 2c, similar to the NIED solution. Dziewonski *et al.* (1991) obtained a dip-slip reverse-faulting mechanism referred to as HRV CMT shown in Figure 2d from the centroid-moment tensor inversion using long-period surface waves. The abbreviation of these solutions follows that used by Pitarka *et al.* (1994).

Pitarka *et al.* (1994) demonstrated that there is a remarkable difference in simulated near-field strong motions for the four different source mechanisms and concluded that the NIED solution is the most appropriate based on strong-motion waveform modeling. However, the NIED solution is inconsistent with the polarities and waveforms at some stations, as indicated by Ishida and Kikuchi (1992). For example, the polarity of the *P* wave at station Tateyama (TYM) cannot be explained by the NIED solution, as indicated in Figure 2a. The data used to derive the NIED solution may have been insufficient to accurately constrain the solution. The data used in Pitarka *et al.* (1994) were strong-motion records obtained at three stations in the Odawara area that are very close to each other and thus have station azimuths differing by only 17°, less than adequate sampling of the radiation pattern. In addition, they used only the tangential component. Thus, more accurate estimates of the source model can be derived by using three-component waveform data recorded at well-distributed stations.

Strong-Motion Stations and Data

The 1990 Odawara earthquake was recorded by digital strong-motion stations in the southern Kanto district operated by several organizations. In order to investigate a source model of the event, we select three-component waveform data at the following four stations, AJR (epicentral distance $R = 18.5$ km), ASK ($R = 49.9$ km), HNG ($R = 82.0$ km), and KR1 ($R = 7.1$ km) indicated in Table 2 and Figure 1b. Those stations were selected based on the azimuthal coverage (Fig. 2), geological conditions, and data available for

Table 2
Location of Local Stations and Instruments Used in Waveform Modeling for Source Parameters

Station	Abbreviation	Lat. (°N)	Long. (°E)	Distance (km)	Azimuth (°)	Instrument (sensor)*	Organization†
Ajiro	AJR	35.04	139.10	18.5	−178.3	JMA-87 (acceleration)	JMA
Asakawa	ASK	35.64	139.28	49.9	19.1	MRM (velocity)	TIT
Kuno	KR1	35.27	139.13	7.1	16.5	SMAD-3 (acceleration)	ERI
Hongo‡	HNG	35.72	139.76	82.0	46.7	VSE-11 (velocity)	FRI

*Instrument—JMA-87: accelerometer deployed at JMA observatories since 1987 (Kakishita *et al.,* 1992). MRM: velocity seismometer developed by Muramatsu (1977). SMAD-3: accelerometer produced by Akashi-Seisaku-Sho. VSE-11: velocity seismometer produced by Tokyo-Sokushin.

†Organization—JMA: Japan Meteorological Agency. TIT: Tokyo Institute of Technology (Samano and Seo, 1988). ERI: Earthquake Research Institute, University of Tokyo (Kudo *et al.,* 1988). FRI: Fire Research Institute, Ministry of Home Affairs (Zama, 1992).

‡Hongo: This station is located on the campus of the University of Tokyo where seismograms from the 1923 Kanto earthquake were recorded.

constructing crustal structure models including near-surface crustal layers.

Since station AJR, ASK, and KR1 are on shallow or surficial rock, local site effects are expected to be relatively simple compared to those at sediment sites. In addition, results from several previous seismic exploration experiments conducted around these stations are available (see Fig. 1b). In contrast, station HNG at which seismograms from the 1923 Kanto earthquake were recorded is located on a thick sedimentary basin. However, high-quality *P*- and *S*-wave velocity data from the Koto deep well located in the northern waterfront area in Tokyo Bay (see Fig. 1b), as well as the results from seismic refraction surveys carried out in the Tokyo metropolitan area (Research Group on Underground Structure in the Tokyo Metropolitan Area, 1989), have recently become available.

Digital accelerometers were in operation at stations AJR and KR1 during the 1990 Odawara earthquake (Kakishita *et al.,* 1992; Kudo *et al.,* 1988; Subcommittee of Earthquake Data Selection, Japanese Working Group on the Effects of Surface Geology on Seismic Motion, 1992), while digital velocity seismometers were operating at stations ASK and HNG (Samano and Seo, 1988; Zama, 1992) (Table 2). These records were integrated into displacement data.

Forward-Modeling Procedure for Velocity Structure Models

In estimating the source model, we calculate Green's functions that represent path effects assuming a one-dimensional horizontally layered velocity structure. As we describe later, both the uppermost crust and the deeper crust in the southern Kanto district have complex structure. Therefore, we model each source-receiver path individually.

The forward-modeling procedure used to derive velocity structure models involves the following steps. First, we construct an initial velocity model based on detailed knowledge from seismic exploration experiments, travel-time tomography, and geological maps. Second, using the *f-k* method and GRT and assuming a number of focal mechanisms, we do a preliminary analysis of the sensitivity of the synthetic waveforms to the initial model in order to select a working model that has the potential to reproduce the basic features of the observed body waveforms.

If significant multiple-reflection phases following the direct body-wave phase are clearly seen in the observed waveforms, we can also make use of some of those multiples if necessary. If the initial model does not have the potential to reproduce the basic waveforms, we introduce more layers and perturb the velocities and thicknesses of the layers. This procedure is repeated until the initial velocity model becomes the working model. Finally, we tune the working model to obtain a preferred model by trial and error, using absolute and relative times of observed direct *P* and *S* waves (and the first multiples if necessary) on three components. If the velocity structure is not adequate, simultaneous waveform match on all three components cannot be achieved. Accordingly, the validity of the preferred velocity models can best be judged after we have presented the results of the three-component waveform modeling. In the following, we describe how we constructed velocity models for each travel path in more detail.

Deep Crustal Structures

Lees and Ukawa (1992) recently obtained three-dimensional images of *P*- and *S*-wave velocities in the crust and upper mantle using travel-time data from a number of earthquakes. Based on their results in conjunction with the contour maps of the depths of the Conrad and Moho discontinuities (Ashiya *et al.,* 1987; Zhao *et al.,* 1994), we constructed a flat-layered model of the uppermost mantle and crust (except for the near-surface crustal layers) for each source-receiver path. In this procedure, we assigned to each layer the average value of the velocities determined by Lees and Ukawa (1992) over the travel path.

Uppermost Crustal Structure

Station KR1 is located at the western edge of the Ashigara Valley in Odawara city where the most detailed studies on local site effects ever done in Japan were made by the Japanese Working Group on the Effects of Surface Geology on Seismic Motion (JESG). Logging of two boreholes, a seismic refraction survey (see line b in Fig. 1b) and a shallow

reflection survey were conducted there by the Subcommittee for Geotechnical Survey on the Ashigara Valley Blind Prediction Test, JESG (1992). Higashi and Kudo (1992) and Higashi (1994) compiled those data and obtained two- and three-dimensional near-surface crustal profiles. In addition, Miyakoshi *et al.* (1994) inferred *P*- and *S*-wave velocity structure near the station from Rayleigh-wave dispersion characteristics obtained from array measurements of microtremors. We used these results in constructing an initial model. In obtaining the preferred velocity model given in Table 3, we did not need to modify the initial model.

At station AJR in the northeastern part of the Izu peninsula, we constructed an uppermost velocity model based on the results of a seismic refraction survey in the Izu Peninsula (Yoshii *et al.*, 1985) (see line c in Fig. 1b). Although no *S*-wave velocity data around AJR station are available, we inferred them from *S*-wave velocities in the Ashigara Valley described above, assuming geological continuity. We did not need to change the properties of the uppermost crustal layers of the initial model in obtaining the working model, but we tuned the thicknesses of these layers based on relative travel times of the observed *P* and *S* waves in order to obtain the preferred model given in Table 3.

For station ASK, we constructed an initial model based on a *P*-wave velocity profile obtained from a seismic refraction survey in the western part of the Tokyo metropolitan area (Yamanaka *et al.*, 1993) and *S*-wave velocities obtained from the Fuchu deep well drilled to a depth of 3 km, which is located about 10 km east of the station (Yamamizu *et al.*, 1981; Asano *et al.*, 1991) (see line a and the solid triangle labeled Fuchu in Fig. 1b). However, this model could not reproduce the basic features of the observed *SV* waveforms on the radial and vertical components for any focal mechanism. Considering the complexity of the travel-time data in the refraction survey (Yamanaka *et al.*, 1993), and the sensitivity of *SV* waveforms to receiver structure (Saikia and Herrmann, 1987; Helmberger *et al.*, 1993), we divided the intermediate layer into two layers. Consequently, the four-layer model became a working model. The preferred model is given in Table 3.

For station HNG, first we extracted layer interfaces with high impedance contrast and average *P*- and *S*-wave velocities for each layer at the Koto deep well drilled to a depth of 3 km (Suzuki, 1993, 1995; Yamamizu *et al.*, 1995) in the northern margin of Tokyo Bay, which is located about 10 km south of station HNG (see the solid triangle labeled Koto in Fig. 1b). This deep well is the closest to station HNG of the four deep wells deployed in the Tokyo metropolitan area. The depths of the layer interfaces beneath station HNG were interpolated based on contour maps of the depths of geological layers (Kawai, 1965; Kakimi, 1973; Minashi *et al.*, 1979) and two- or three-dimensional velocity profiles obtained from a series of seismic refraction surveys conducted in the Tokyo Metropolitan area (Research Group on Underground Structure in the Tokyo Metropolitan Area, 1989; Koketsu and Higashi, 1992). For the surface layer, we used the logging data in a borehole drilled to a depth of about 80 m at station HNG (Tanaka *et al.*, 1973). We did not need to change the seismic parameters of the uppermost crustal layers of the initial model in obtaining the working model, but we slightly tuned the thicknesses of these layers based on the relative travel times of the observed *P* and *S* waves and subsequent multiples in order to obtain the preferred model given in Table 4. The validity of this model is discussed further with the final results.

Table 3
Velocity Structure Models for Local Stations AJR, ASK, and KR1 on Rock

Station	Depth* (km)	Thickness (km)	*Vp* (km/sec)	*Vs* (km/sec)	ρ (g/cc)	*Qp*	*Qs*
AJR	0.0	0.3	2.60	1.30	2.3	100	50
	0.3	0.7	4.20	2.40	2.5	150	75
	1.0	1.0	5.30	3.12	2.6	300	150
	2.0	3.0	5.60	3.26	2.6	300	150
	5.0	5.0	6.10	3.53	2.6	300	150
	10.0	5.0	6.40	3.70	2.7	300	150
	15.0	—	6.90	3.92	2.9	500	250
ASK	0.0	0.2	3.00	1.40	2.3	150	75
	0.2	1.1	4.70	2.40	2.5	200	100
	1.3	2.7	5.00	2.90	2.5	300	150
	4.0	1.0	5.60	3.26	2.6	300	150
	5.0	10.0	6.30	3.64	2.7	300	150
	15.0	—	6.90	3.92	2.9	500	250
KR1	0.0	0.25	2.20	0.70	2.1	100	50
	0.25	1.0	3.00	1.50	2.3	150	75
	1.25	0.75	4.20	2.40	2.4	200	100
	2.0	3.0	5.60	3.26	2.6	300	150
	5.0	5.0	6.10	3.53	2.6	300	150
	10.0	5.0	6.40	3.70	2.7	300	150
	15.0	—	6.90	3.92	2.9	500	250

*Depth to the top of the layer.

Table 4
Velocity Structure Model for Local Station HNG on Sediments

Station	Depth* (km)	Thickness (km)	*Vp* (km/sec)	*Vs* (km/sec)	ρ (g/cc)	*Qp*	*Qs*
HNG	0.0	0.1	1.80	0.40	1.8	40	20
	0.1	0.2	1.90	0.80	1.9	60	30
	0.3	0.3	2.20	1.15	2.0	100	50
	0.6	0.6	2.30	1.20	2.0	100	50
	1.2	0.8	2.70	1.30	2.1	150	75
	2.0	0.5	3.30	1.40	2.3	150	75
	2.5	0.5	4.70	2.72	2.5	300	150
	3.0	9.0	5.70	3.33	2.6	300	150
	12.0	8.0	6.60	3.71	2.8	500	250
	20.0	5.0	6.70	3.74	2.8	500	250
	25.0	9.0	7.00	3.93	3.0	500	250
	34.0	—	7.90	4.44	3.2	1000	500

*Depth to the top of the layer.

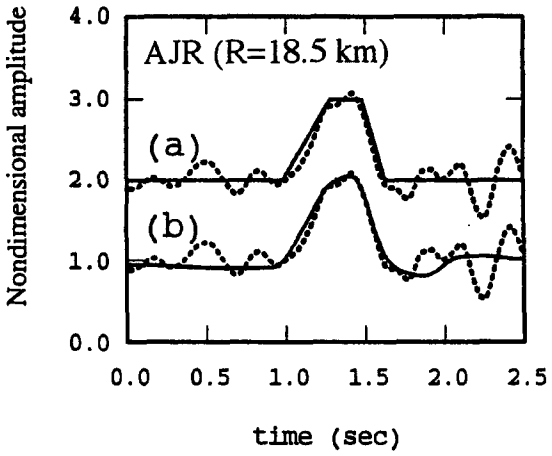

Figure 3. Comparison of observed displacement *SH*-waveform data (dashed line) on the transverse component at AJR station (R = 18.5 km) with the trapezoidal source-time function described by (0.3, 0.2, and 0.15 sec) (a), and the *f-k* synthetic seismogram (b). The *f-k* synthetic seismogram is calculated using the best-fit source model (Sato solution) given in Table 1 and the flat-layered velocity model for AJR station listed in Table 3. The observed and *f-k* synthetic seismograms are bandpass filtered from 0.1 to 10 Hz.

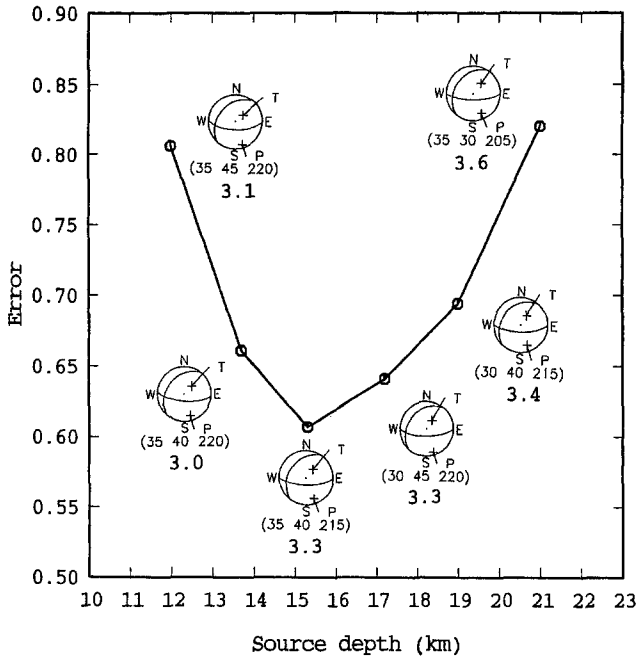

Figure 4. Error as a function of source depth. The source mechanisms are represented by dip, slip, and strike at each depth. The number below each mechanism indicates the seismic moment in 10^{23} dyne-cm. The best fit occurs at a depth of 15.3 km.

Source-Time Function

Station KR1 (epicentral distance R = 7.1 km), which is the closest to the source in this study, does not seem to be suitable to use to obtain source-time function because it is located near nodal planes of both *P* and *SH* waves for all the source mechanisms obtained from the previous studies, as indicated by Figure 3 in Pitarka *et al.* (1994). However, station AJR (R = 18.5 km) is distant from *SH* nodal planes for all of these mechanisms, so we used the transverse-component displacement waveform at station AJR to estimate the source-time function. The data were bandpass filtered from 0.1 to 10 Hz considering the noise level.

Figure 3a compares the observed direct *SH*-wave pulse with a trapezoidal source-time function with 0.30 sec of rise time, 0.20 sec of follow-on time, and 0.15 sec of healing time, found by trial and error. A good fit is obtained. We checked this result by comparing the data with the synthetic seismograms computed by the *f-k* method (see Fig. 3b), using the preferred velocity structure (Table 3) and the best-fit source mechanism after we obtained the final results on the source model. Good agreement in waveforms is obtained for all the cases. This indicates that the direct *SH* wave at station AJR is a good approximation to the source-time function. The estimated source duration of 0.65 sec is longer than that of 0.4 sec estimated by Ishida and Kikuchi (1992) and the 0.5-sec duration estimated by Pitarka *et al.* (1994) (Table 1).

Estimation of Source Model by Grid-Search Technique Using Body-Waveform Data

The displacement seismograms at stations AJR, ASK, KR1, and HNG were bandpass filtered from 0.1 to 1.0 Hz to reduce noise as well as contamination from high-frequency features due to small-scale velocity heterogeneity. In estimating a source model by waveform modeling, we used only the body-wave portion, including both the *P*- and *S*-wave arrivals (see the portions denoted by dotted lines in Fig. 5), since surface waves are too sensitive to lateral heterogeneity of the velocity structure (e.g., Dreger and Helmberger, 1991, 1993). Our source estimation method is based on the direct grid-search technique developed by Zhao and Helmberger (1994), except that we estimated the seismic moment using amplitudes of the whole waveform and not just peak amplitudes (Walter, 1993). The synthetics were aligned with the data based on time shifts calculated by cross-correlation. In this method, the five unknowns determined are the dip, rake, and strike of the fault plane, and depth and seismic moment.

We used the epicenter estimated by Ishida and Kikuchi (1992) listed in Table 1. A set of fundamental Green's functions for the velocity structure models given in Tables 3 and 4 was computed up to 2 Hz for source depths of 11, 13.7, 15.3, 17.2, 19.0, and 21.0 km using the *f-k* method (Saikia, 1994), convolved with the source-time functions estimated earlier, and then bandpass filtered from 0.1 to 1.0 Hz. The direct grid search was performed over 5° increments in dip,

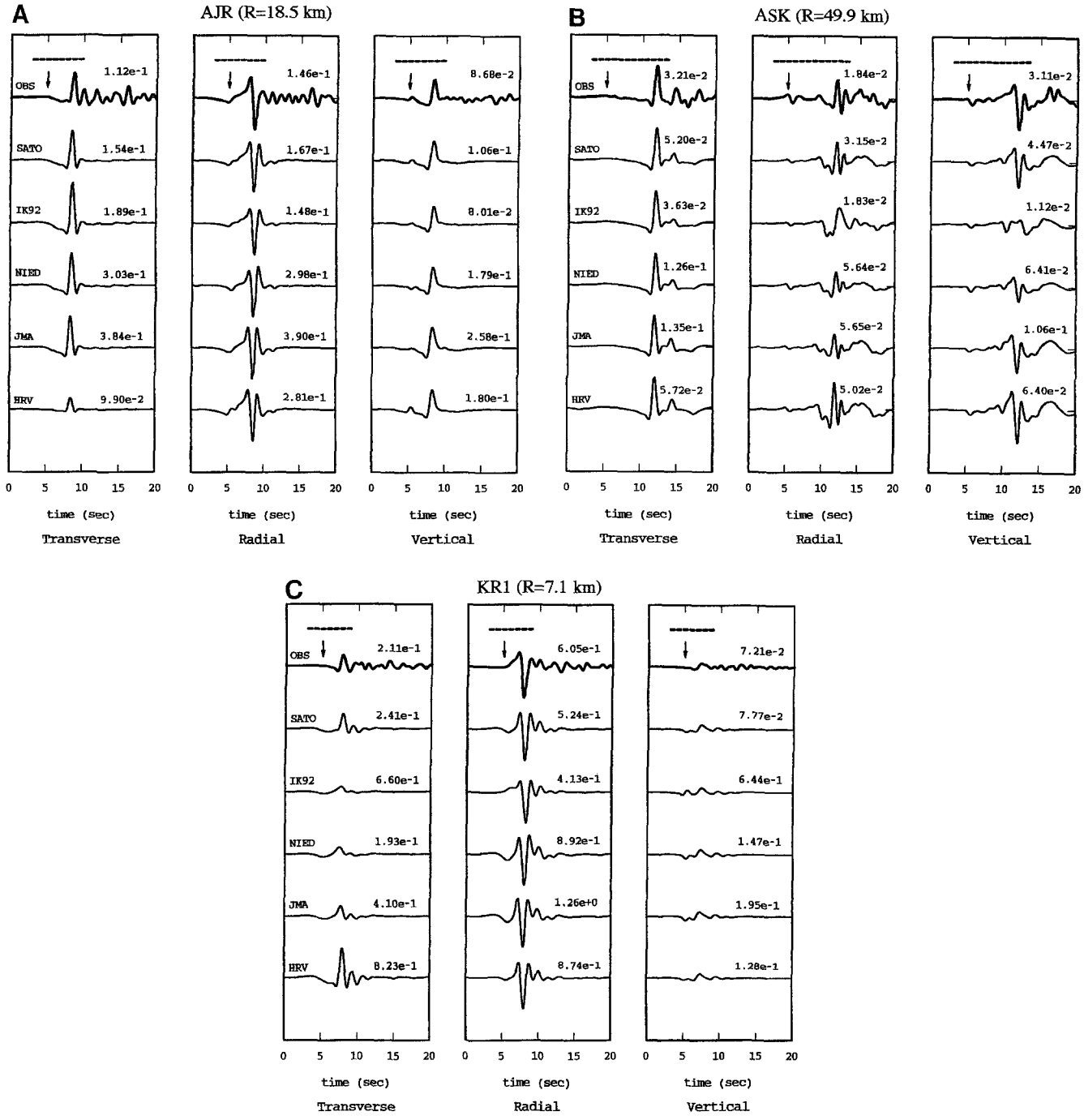

Figure 5. (a) Comparison between the ground displacement waveform data and the *f-k* synthetic waveforms with the various focal mechanisms given in Table 1 at station AJR (R = 18.5 km). Synthetic seismograms with various focal mechanisms are calculated with the corresponding depth and seismic moment given in Table 1. Both the observed and synthetic waveforms are bandpass filtered between 0.1 and 1.0 Hz. The amplitude of each trace is normalized by the maximum amplitude of the corresponding radial component in order to facilitate comparison of the amplitude ratios between three components. The absolute peak amplitudes are indicated on the right of each trace in centimeters. The data and synthetics are aligned with the first *P*-wave arrival indicated by the arrows. The dashed lines above the observed data show the time window used in the grid search in this study. (b) Results at station ASK (R = 49.9 km). The amplitude of each trace is normalized by the maximum amplitude of the corresponding transverse component. (c) Results at station KR1 (R = 7.1 km). The amplitude of each trace is normalized by the maximum amplitude of the corresponding radial component. (d) Results at station HNG (R = 82.0 km). The amplitude of each trace is normalized by the maximum amplitude of the corresponding radial component.

(illustration continued on following page)

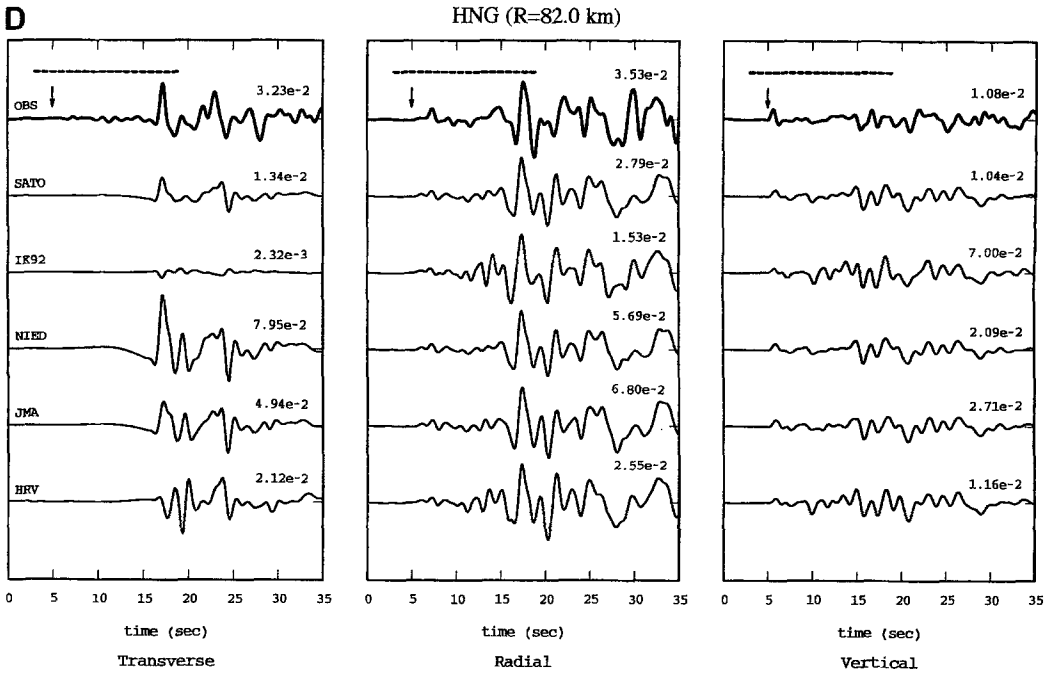

Figure 5. (*Continued*)

Table 5a

Cross-Correlation Coefficients between the Data and Synthetics for Various Source Models

Station Name Epicentral Distance (km) Component	AJR 18.5			ASK 49.9			KR1 7.1			HNG 82.0		
	T	*R*	*V*	*T*	*R*	*V*	*T*	*R*	*V*	*T*	*R*	*V*
SATO	0.97	0.92	0.98	0.97	0.94	0.95	0.87	0.92	0.93	0.86	0.86	0.70
IK92	0.97	0.92	0.97	0.97	0.63	0.54	0.63	0.98	0.85	0.58	0.79	0.60
NIED	0.97	0.88	0.97	0.97	0.92	0.95	0.63	0.87	0.88	0.84	0.86	0.69
JMA	0.97	0.91	0.98	0.97	0.94	0.95	0.72	0.89	0.90	0.85	0.86	0.69
HRV CMT	0.95	0.92	0.98	0.97	0.93	0.95	0.92	0.91	0.94	0.39	0.81	0.63

Table 5b

Time Shifts between the Data and the Synthetics for the Best-Fit Source Model (Sato Model)

Station Name Epicentral Distance (km) Component	AJR 18.5			ASK 49.9			KR1 7.1			HNG 82.0		
	T	*R*	*V*	*T*	*R*	*V*	*T*	*R*	*V*	*T*	*R*	*V*
Time shift (sec)*	−0.16	−0.10	−0.06	0.06	0.03	0.06	−0.22	−0.14	−0.18	−0.44	−0.54	−0.34
Time shift (sec)*†	0.01	0.07	0.11	0.23	0.20	0.23	−0.05	0.03	0.01	−0.27	−0.37	−0.17

*The origin time of 1990/8/5 7:13:01.69 sec (GT) estimated by NIED is used. The positive time shift means that synthetics have been delayed.

†The time shifts are estimated based on an assumed origin time of 1990/8/5 7:13:01.86 sec that is calculated by the average time shift of 0.17 sec over the four stations associated with the NIED origin time.

rake, and strike for the whole parameter space. This search was applied in turn to the six source depths described earlier in order to obtain the best-fit solution.

As shown in Figure 4, errors are small in the depth range of 13.7 to 17.2 km, which corresponds to the source depths derived from the previous studies listed in Table 1. The minimum error is obtained at a depth of 15.3 km with a dip of 35°, a rake of 40°, a strike of 215°, and a seismic moment of 3.3×10^{23} dyne-cm. The best-fit solution obtained in this study (Sato solution) is summarized in Figure 2 and Table 1 with the previous source models. The Sato solution is intermediate between two previous solutions: the strike-slip NIED solution and the dip-slip IK92 solution. The estimated seismic moment of 3.3×10^{23} dyne-cm is consistent with

the value of 3.5×10^{23} dyne-cm estimated by Ishida and Kikuchi (1992) but is only half the value of 6.7×10^{23} dyne-cm estimated by Pitarka *et al.* (1994).

For rupture on a circular fault, the source duration is proportional to the radius divided by the shear-wave velocity (Brune, 1970, 1971). The source duration can be written as $\tau = 2.69a/Vs$, and the stress drop for a circular fault can be written as $\Delta\sigma = 7\ M_0/16a^3$, where M_0 is the seismic moment, a is the radius of the circular fault, and Vs is the shear-wave velocity in the vicinity of the source. If we use the Vs of 3.92 km/sec given in Table 3 for the source region (Lees and Ukawa, 1992) and use the parameters obtained in this study, an area of about 2.8 km^2 and a stress drop of 170 bars are obtained. This value is lower than that of 880 bars estimated by Ishida and Kikuchi (1992) and is consistent with the typical value of the local maximum stress drop, 200 bars, but higher than the typical value for subduction zone earthquakes, 30 bars (Kikuchi and Fukao, 1987).

Figure 5 compares the displacement waveform data with the synthetics. The synthetics were computed using the source parameters listed in Table 1, except that the epicenter estimated by Ishida and Kikuchi (1992) was applied to all the source models. In Figure 5, amplitudes of the three-component seismograms are normalized by the peak amplitude of a reference-component seismogram in order to facilitate comparison of the amplitude ratios between the three components. The radial component is used as the reference component at stations AJR, KR1, and HNG, and the transverse component is used at ASK. The numbers on the right side of the seismograms indicate the absolute peak amplitudes in centimeters. All the waveforms are aligned with the first *P*-wave arrival at 5 sec on the time axes. Table 5a lists the

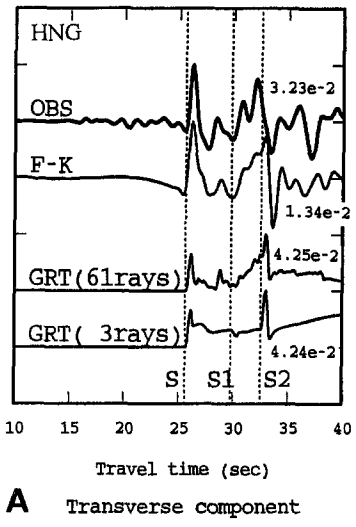

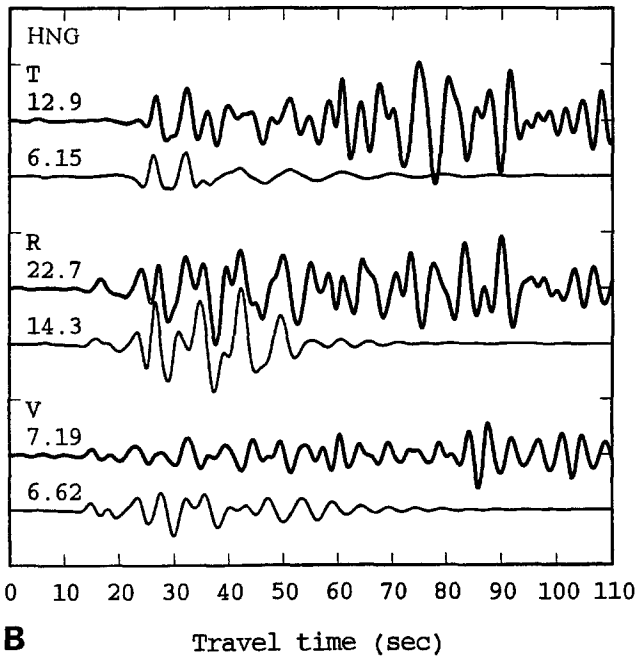

Figure 6. (a) Comparison of the tangential displacement waveform data (top trace) with the synthetic waveforms (second through fourth traces) at station HNG (R = 82.0 km). The synthetic seismograms are calculated using the best-fit source model (Sato solution) in Table 1 and the velocity model in Table 4. The second trace is calculated by the *f-k* method. Both the first and second traces are bandpass filtered between 0.1 and 1.0 Hz. The third and fourth traces are computed using GRT. No filter is applied to the GRT synthetic seismograms in order to show the arrivals of specific phases. In the third trace, the responses of all 61 rays, which departed upward and were reflected up to twice, are included. In the fourth trace, three rays that are the direct *SH* wave (*S*), and two multiple reflections (*S*1 and *S*2) are included. *S*1 is the arrival time of the ray that departed upward from the source and was reflected between the free surface and the top of the granitic layer at a depth of 2.5 km. *S*2 is the arrival time of the ray that departed upward from the source and was reflected between the free surface and the Conrad discontinuity at a depth of 12 km. Each seismogram is scaled to its maximum amplitude. (b) Comparison between the three-component, whole waveform displacement data with the synthetic waveforms at HNG station (R = 82.0 km). The upper traces are the observed waveforms. The lower traces are the synthetic waveforms computed by the *f-k* method. The bandpass filter from 0.10 to 0.33 Hz is applied to both the data and the synthetics. The numbers above the traces are the absolute peak amplitudes in 10^{-3} cm.

cross-correlation coefficients between the displacement waveform data and the synthetic waveforms for the various source mechanisms. The synthetics for the source model obtained in this study show the best agreement with the data in terms of waveforms, amplitude ratios, amplitudes, and the cross-correlation coefficients at all the stations. The dip-slip type IK92 and HRV CMT solutions cannot reproduce basic features of the data at some stations. For example, the IK92 solution fails to explain the waveform data on the radial and vertical components at ASK (Fig. 5b and Table 5a), and the polarity of the transverse component at HNG (Fig. 5d and Table 5a) is opposite to the data at HNG. The polarity of the *SH* wave at HNG for the HRV CMT solution is also inconsistent with that of the data (Fig. 5d and Table 5a). The dip-slip solutions NIED and JMA reproduce the polarities as well as the basic features of the waveform data at all four stations. However, the agreement in amplitude ratios and the cross-correlation coefficients are not as good as that for the best-fit solution. Moreover, at station TYM, the solutions NIED and JMA fail to explain the *P*-wave polarity data, while the best-fit solution is consistent with the polarity data as indicated in Figure 2e.

For the best-fit solution, a surprisingly high correlation is obtained on all three components at ASK (Table 5a), considering that we assumed one of the near-surface layers in deriving the working velocity model. Table 5b lists the time shifts between the data and the synthetic seismograms for the best-fit solution. If we obtain an appropriate origin time assuming that the preferred velocity models are accurate, it would be delayed by about 0.17 sec with respect to the NIED origin time. This delay seems to be reasonable because it is smaller than that of 0.5 sec for the JMA origin time with a depth of 13.7 km. However, this may not be pertinent since the time shifts are not the same at all the stations. The deviation of the time shifts indicates misfit in the preferred velocity models. If we assume that the preferred velocity models for stations AJR and KR1 are more accurate than those for stations ASK and HNG, the bottom row of Table 5b indicates that the velocities of the preferred model for ASK should be faster but that the velocities of the preferred model for HNG should be slower. However, the deviation of the time shift of 0.3 to 0.4 sec is not large considering the relatively large epicentral distances at stations ASK (R = 49.9 km) and HNG (R = 82.0 km). In addition, at station HNG, synthetic later phases including multiple reflections and surface waves, which are not used in the grid-search procedure, fit the data well, as seen in Figures 5b and 5d. Hence, we conclude that the preferred flat-layered velocity structure models are adequate for source retrieval.

Later Phases at Station HNG

Several researchers (e.g., Yamanaka *et al.*, 1992; Kato *et al.*, 1993; Hisada *et al.*, 1993) investigated ground-motion characteristics observed at sites in the Tokyo metropolitan area from the shallow Izu earthquakes (Fig. 1b) and pointed out that observed surface waves from the Izu earthquakes are strongly affected by near-source heterogeneity in a Quaternary basin in Sagami Bay (Nishizawa *et al.*, 1996). However, considering the geometrical relationship between the location of the major asperities of the 1923 Kanto earthquake derived by Wald and Somerville (1995) and the location of Sagami Bay (Fig. 1b), it appears that the ground motions in the Tokyo metropolitan area from the 1923 Kanto earth-

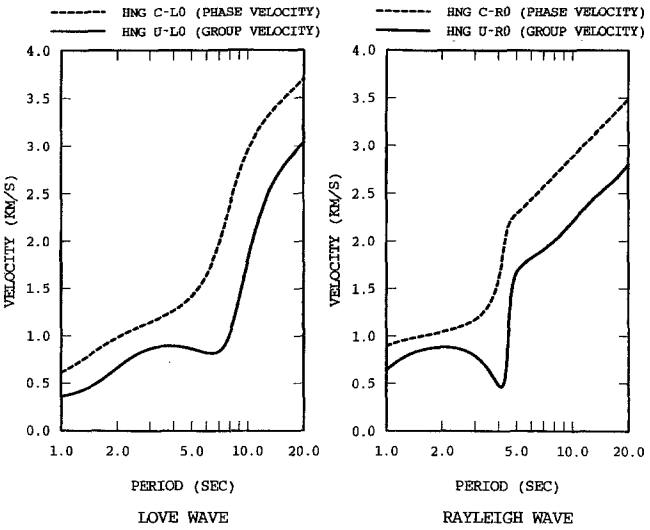

(a) Dispersion curves

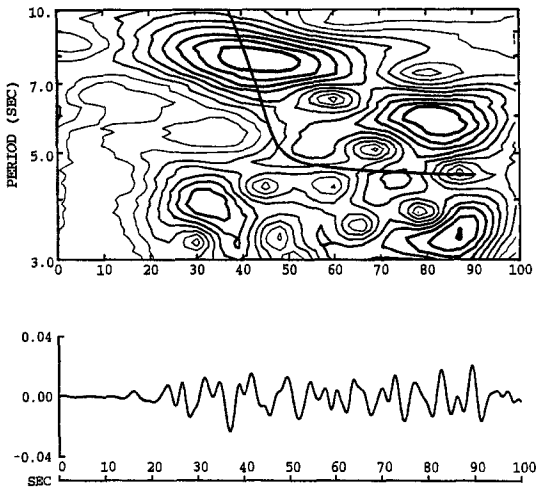

(b) Dispersion characteristics (Radial component)

Figure 7. (a) Theoretical dispersion curves of the fundamental-mode Love (L0) and Rayleigh (R0) waves for the velocity model for station HNG given in Table 4. The dotted lines represent phase velocity, and the solid lines represent group velocity. (b) Dispersion characteristics of the observed radial-component displacement motion at station HNG (R = 82.0 km). The nonstationary spectrum is calculated by the multiple-filter technique. The solid line denotes the group delay time of the fundamental-mode Rayleigh wave for the velocity model given in Table 4. The origin time is assumed to be 7:13:01.69 sec (GT).

Table 6
Location of Regional Stations and Instruments Used in Waveform Modeling for Propagation Paths

Station	Abbreviation	Lat. (°N)	Long. (°E)	Distance (km)	Azimuth (°)	Instrument*	Organization†
Inuyama	INU	35.34	137.02	190.3	−85.2	STS-1 (velocity)	NGU
Gifu‡	GIF	35.40	136.77	213.7	−83.7	JMA-59 (displacement)	JMA
Sendai§	SND	38.26	140.90	374.6	24.8	JMA-59 (displacement)	JMA

*Instrument—STS-1: Streckeisen STS-1 broadband velocity seismometer. JMA-59: conventional paper-recording displacement seismometer deployed at JMA observatories since 1959.

†Organization—NGU: Nagoya University (Yamada *et al.*, 1989). JMA: Japan Meteorological Agency.

‡Gifu: Seismograms from the 1923 Kanto earthquake were recorded at this station.

§Sendai: Seismograms from the 1923 Kanto earthquake were recorded at the Mukaiyama observatory of Tohoku University, which is located about 4 km southwest of this JMA Sendai station.

quake may not be affected strongly by the heterogeneity of Sagami Bay.

Little research on wave propagation characteristics from earthquakes occurring in the source region of the 1923 Kanto earthquake has been done because no moderate- or large-sized modern earthquakes had occurred in the region until the 1990 Odawara earthquake. Therefore, examining the validity of the flat-layered model in relation to the later phases at HNG from the 1990 event will provide us with an indication of the reproducibility of observed significant later phases at station HNG during the 1923 Kanto earthquake when we use the flat-layered model (Table 4) in the companion article (Sato *et al.*, 1998).

In order to examine obvious pulses arriving after the direct *SH* wave on the transverse component at station HNG (Fig. 5d), we generated synthetic seismograms by *f-k* and GRT using the flat-layered model given in Table 4 and then compared them with the data, as shown in Figure 6a. We applied a bandpass filter from 0.1 to 1.0 Hz to both the data and the *f-k* synthetics but did not apply the bandpass filter to the GRT synthetics in order to show the arrivals of specific phases. The second trace, an *f-k* synthetic seismogram, shows good agreement with the data. The third trace is a GRT synthetic seismogram constructed using all 61 rays that are radiated upward from the source and then reflected twice at the interfaces of the layers. The fourth trace is a GRT synthetic using only three rays, namely, the direct arrival (*S*), the multiple reflection between the free surface and the top of the basement at a depth of 2.5 km (*S*1), and the multiple reflection between the free surface and the Conrad discontinuity at a depth of 12 km (*S*2). The comparison reveals that the observed significant pulselike later phase at about 33 sec in Figure 6a following the direct *SH* wave is contributed by the multiple reflection (*S*2) in the upper crust.

At HNG, later phases with long duration are also seen in the data. Figure 6b compares the three-component waveform data with synthetic seismograms calculated by the *f-k* method using the flat-layered model given in Table 4 in the frequency range of 0.10 to 0.33 Hz. The velocity model works well for about the first 40 sec after the first *P*-wave arrival on the radial component but does not reproduce the following later phases nor arrivals after the first 20 sec on the transverse and vertical components. We analyzed the observed dispersion characteristics of the later phases using a multiple filter technique (Dziewonski *et al.*, 1969). Figure 7b compares the observed dispersion characteristics of the radial component, on which the later phases are predominant for the first 30 sec after the *S*-wave arrival, with the theoretical group delay time of the fundamental-mode Rayleigh wave (Fig. 7a) for the velocity model given in Table 4. A reasonable fit is obtained at periods longer than about 7 sec for the first 30 sec after the *S*-wave arrival.

These results indicate that the flat-layered model for HNG given in Table 4 is effective not only for modeling body waves but also for the early part of the surface waves for the 1990 Odawara earthquake at periods longer than 3 sec. They also imply that this velocity model has the potential to simulate waveforms due to body waves and direct surface waves at station HNG from the 1923 Kanto earthquake, based on

Table 7
Velocity Structure Models for Stations INU and GIF

Model	Depth* (km)	Thickness (km)	*Vp* (km/sec)	*Vs* (km/sec)	ρ (g/cc)	*Qp*	*Qs*
LU	0.0	4.0	5.50	3.25	2.6	300	150
	4.0	20.0	6.11	3.61	2.7	300	150
	24.0	10.0	7.15	4.01	3.0	500	250
	34.0	—	7.81	4.41	3.2	1000	500
LI	0.0	3.0	5.30	3.14	2.6	300	150
	3.0	15.0	6.00	3.55	2.7	300	150
	18.0	15.0	6.80	3.82	2.8	500	250
	33.0	—	7.60	4.29	3.1	1000	500
LS	0.0	1.5	4.00	2.07	2.4	200	100
	1.5	1.5	4.70	2.72	2.5	300	150
	3.0	3.0	5.60	3.29	2.6	300	150
	6.0	7.0	6.20	3.58	2.7	300	150
	13.0	6.0	6.30	3.64	2.8	300	150
	19.0	10.0	6.80	3.80	2.9	500	250
	29.0	5.0	6.90	3.90	3.0	500	250
	34.0	—	7.30	4.12	3.1	1000	500

*Depth to the top of the layer.

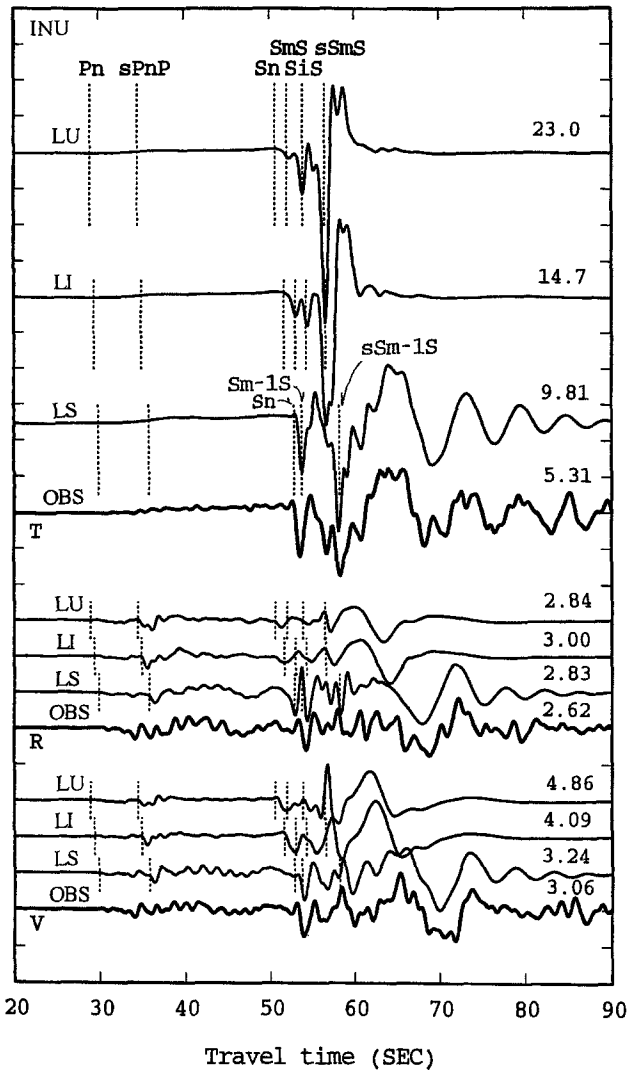

Figure 8. Comparison between the three-component, whole waveform data with the synthetic waveforms for the various velocity models given in Table 7 at station INU (R = 190 km). The top traces are for the velocity model LU; the second ones are for the model LI; the third ones are for the model LS obtained in this study; the bottom ones are observed. A bandpass filter from 0.02 to 1.0 Hz is applied to both of the data and synthetics. The numbers on the right of each trace are the absolute peak amplitudes in 10^{-3} cm. The origin time is assumed to be 7:13:01.69 sec (GT). The arrival times of the phases *Pn, sPnP, Sn, SmS, SiS,* and *sSmS* are plotted on the synthetic seismograms for the velocity models LU and LI. On the synthetic seismograms for the velocity model LS, the phase *Sm-1S* that is reflected from the upper boundary of the layer with an *S*-wave velocity of 3.9 km/sec and the corresponding depth phase *sSm-1S* are plotted in addition to the phases *Pn, sPnP,* and *Sn.*

the analogy between the travel paths from the major asperities (Wald and Somerville, 1995) and from the 1990 Odawara earthquake. However, modeling the later phases following the direct surface waves using the flat-layered model proves ineffective and requires a two- or three-dimensional crustal model including the sedimentary basin (e.g., Kudo, 1980; Liu and Heaton, 1984; Vidale and Helmberger, 1988; Yamanaka *et al.,* 1989, 1992; Toshinawa and Ohmachi, 1992; Kato *et al.,* 1993; Hisada *et al.,* 1993; Graves, 1993). This problem will be addressed in future work.

Waveform Modeling at Regional Stations

During the 1923 Kanto earthquake, relatively good-quality horizontal and vertical seismograms were obtained at station GIF, which is located about 220 km west of the epicenter (Fig. 1a). Therefore, it is important to estimate wave propagation path effects from the source region of the 1923 Kanto earthquake to station GIF. At this station, seismograms from the 1990 Odawara earthquake were also recorded by a JMA-59 type seismograph, which is a conventional electro-magnetic paper-recording seismograph (Table 6). The instrument constants of the JMA-59 type seismograph are T_0 (natural period) = 5 sec, h (damping constant) = 0.5, and v (magnification) = 100. In addition, high-quality data from the 1990 Odawara earthquake were recorded by broadband STS-1 seismometers (T_0 = 360 sec, h = 0.707) at the Inuyama observatory (INU) of Nagoya University, which is located about 20 km east of GIF station (Yamada *et al.,* 1989) (see Fig. 1a and Table 6). Geologically, INU is a rock site, and most of the area between the epicenter of the 1990 Odawara earthquake and INU is exposed rock.

So far, numerous studies have demonstrated the effectiveness of broadband data for understanding the role of crustal structure in influencing regional and local ground motions (e.g., Helmberger *et al.,* 1992b, 1993). Accordingly, we first use the broadband data from the 1990 Odawara earthquake to model the travel path from the southern Kanto district to station INU using a flat-layered model and then examine the adequacy of the velocity model for explaining the ground motions at station GIF, which is on thin sediments (Masaki and Iida, 1981, 1982; Sasaki *et al.,* 1984).

Waveform Modeling at Station INU

Ukawa and Fukao (1981) determined one-dimensional *P*- and *S*-wave velocity structures beneath central Honshu, Japan, by the inversion of travel-time data from crustal and subcrustal earthquakes occurring in and around the Nagoya University Telemeter Network. They also pointed out that the *Vp/Vs* ratio of the upper crust is about 1.69, while it is 1.77 to 1.78 in the lower crust and the sub-Moho mantle. Based on their results, we constructed a flat-layered model called LU listed in Table 7. Ikami (1978) obtained a *P*-wave velocity profile along Sagami Bay to Inabu located about 50

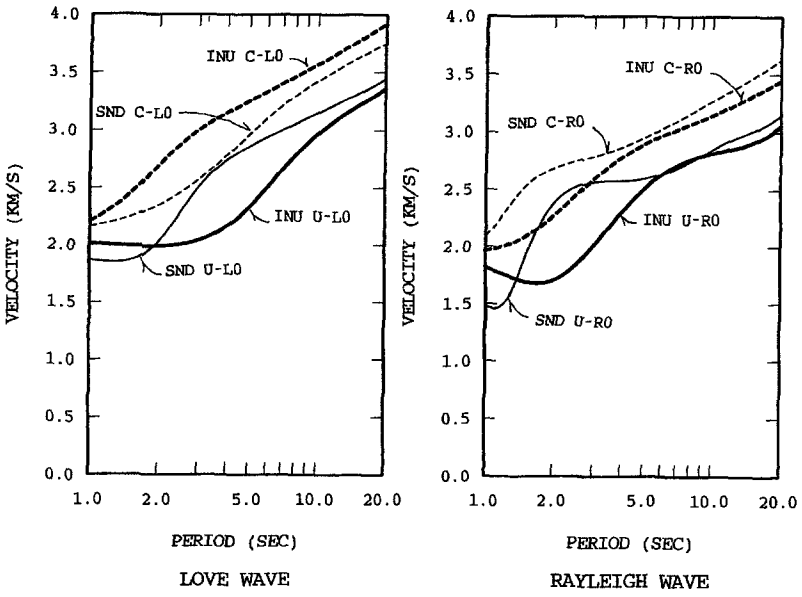

Figure 9. Theoretical dispersion curves of the fundamental-mode Love and Rayleigh waves for velocity model LS for station INU in Table 7 and the velocity model for station SND in Table 8. The dotted and solid lines represent the phase and group velocities, respectively.

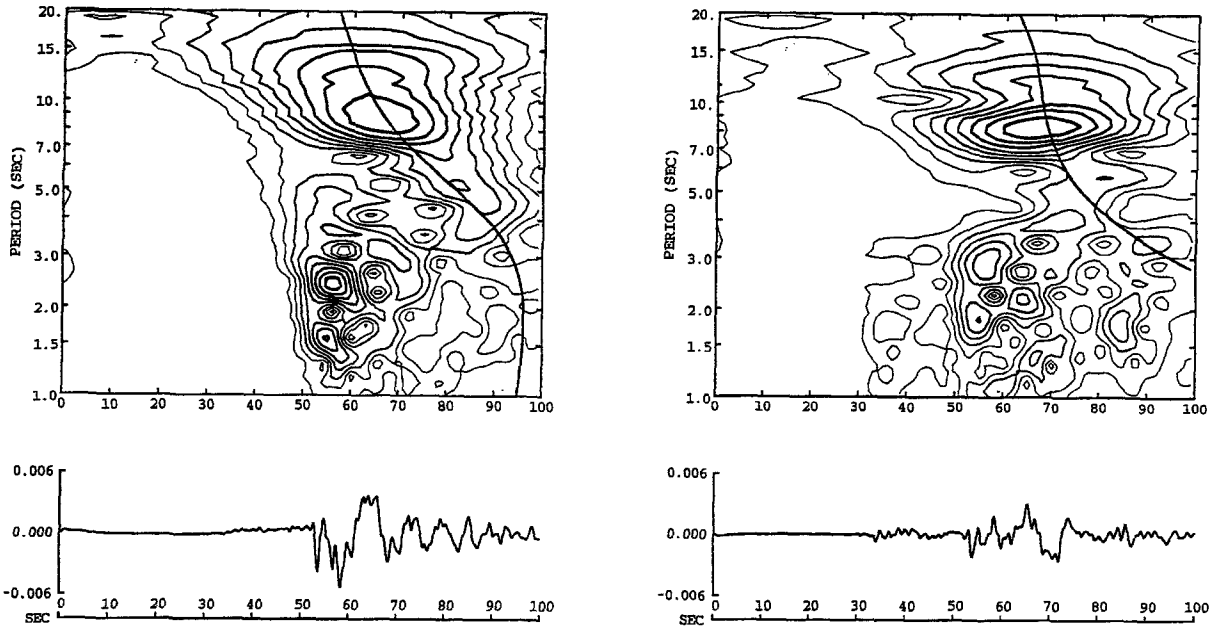

(a) Transverse component (b) Vertical component

Figure 10. (a) Dispersion characteristics of the observed transverse-component displacement motion at station INU (R = 191 km). The nonstationary spectrum is calculated by the multiple-filter technique. The solid line denotes the group delay time of the fundamental-mode Love wave for velocity model LS given in Table 7. The origin time is assumed to be 7:13:01.69 sec (GT). (b) Dispersion characteristics of the observed vertical-component displacement motion at station INU. The solid line denotes the group delay time of the fundamental-mode Rayleigh wave for velocity model LS given in Table 7.

km southeast of INU (see line b in Fig. 1a) from a seismic refraction survey. Based on the P-wave velocity profile around Inabu and the Vp/Vs ratios derived by Ukawa and Fukao (1981), we constructed a flat-layered model called LI listed in Table 7. Based on waveform modeling, we constructed another flat-layered model called LS listed in Table 7.

First, we compare the observed displacement waveforms bandpass filtered from 0.02 to 1.0 Hz with synthetic seismograms for the velocity models LU and LI calculated

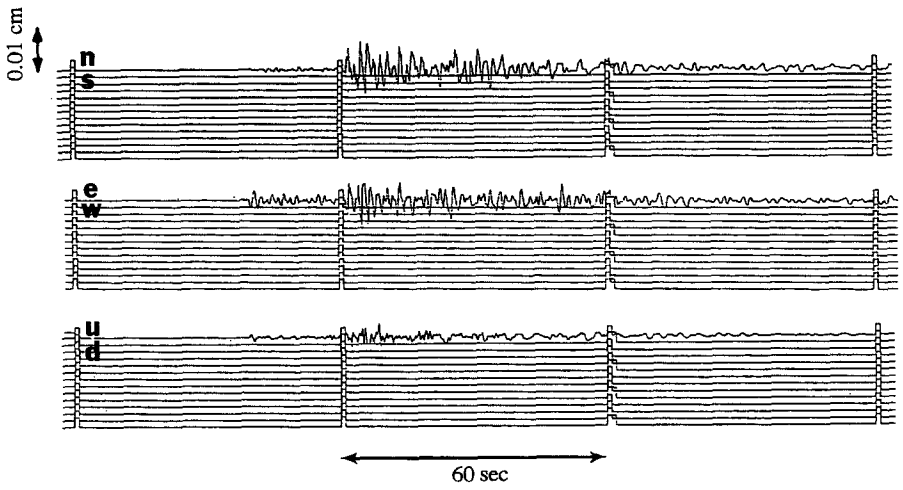

Figure 11. The seismogram recorded by the JMA-59 type seismograph at station GIF (R = 214 km).

by the *f-k* method using the best-fitting source model obtained in this study (Fig. 8). The waveforms are plotted in absolute time with the NIED origin time listed in Table 1. On the radial and vertical components, the basic features of the *Pnl* waves (Helmberger and Engen, 1980) in the synthetic seismograms for models LU and LI are somewhat different from those in the data. This discrepancy indicates inconsistency in the crust and uppermost mantle structures in an average sense. On the transverse component, the arrivals of the *Sn* (mantle head wave), *SmS* (reflection from the Moho), *SiS* (reflection from the Conrad), and *sSmS* (depth phase from the Moho) in the synthetic seismograms for velocity models LU and LI are about 1 or 2 sec faster than the data. This difference in arrival times is larger than the uncertainty in origin time of about 0.5 sec, as indicated in Table 1. The relative strengths of these *SH* pulses for the synthetics are also different from those in the data. This suggests that the *S*-wave velocities of the lower crust and/or the upper mantle should be slower. Moreover, the synthetic seismograms do not model the well-developed Love waves, and the synthetic Rayleigh waves arrive too early. Since surface waves are strongly controlled by the shallow part of the crust, this suggests that the velocities of the uppermost crust should be slower.

Based on the three-dimensional images of the velocity perturbations (Ishida and Hasemi, 1990; Lees and Ukawa, 1992; Zhao *et al.*, 1994), the shallow seismic refraction experiments conducted in central Honshu (Sasatani *et al.*, 1990; Matsu'ura *et al.*, 1991) (see lines a and c in Fig. 1a), and the *Vp*/*Vs* ratios derived by Ukawa and Fukao (1981), we constructed a new flat-layered model and then tuned the model by trial and error so that both body and surface waveforms were reproduced. In the body-waveform modeling, we focused on relative and absolute travel times and relative amplitudes of the various major phases. In the surface-waveform modeling, we sought to explain the observed dispersion characteristics. As a result, in the period range of 0.02 to 1.0 Hz, the synthetic seismograms with the preferred model listed as model LS in Table 7 successfully reproduce not only the body waves but also the surface waves in terms of travel times, waveform characteristics, relative amplitudes of the various phases, and absolute amplitudes (Fig. 8). The major two *SH* peaks are caused by the reflected phase and the depth

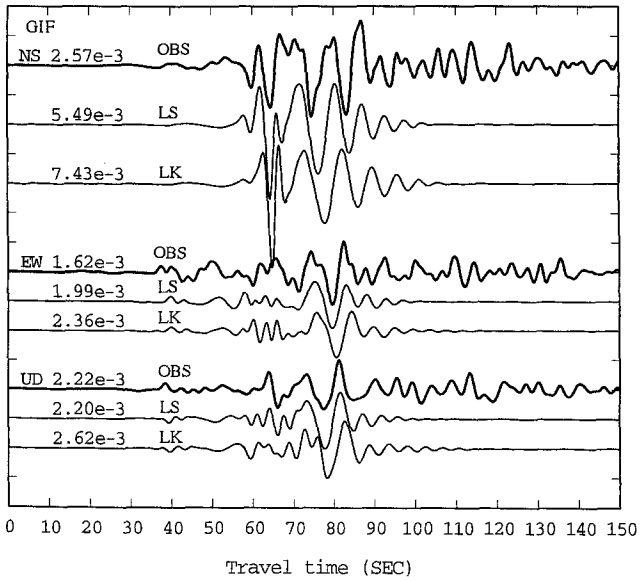

Figure 12. Comparison between the three-component, whole waveform data (top traces) and the synthetic waveforms for velocity model LS (second traces) in Table 7 and velocity model LK (Nozawa *et al.*, 1996) (bottom traces) in Table 10 at station GIF (R = 214 km). A bandpass filter from 0.067 to 0.33 Hz is applied to both the data and synthetics. The numbers above the traces are the absolute peak amplitudes in 10^{-3} cm. The origin time is assumed to be 7:13:01.69 sec (GT).

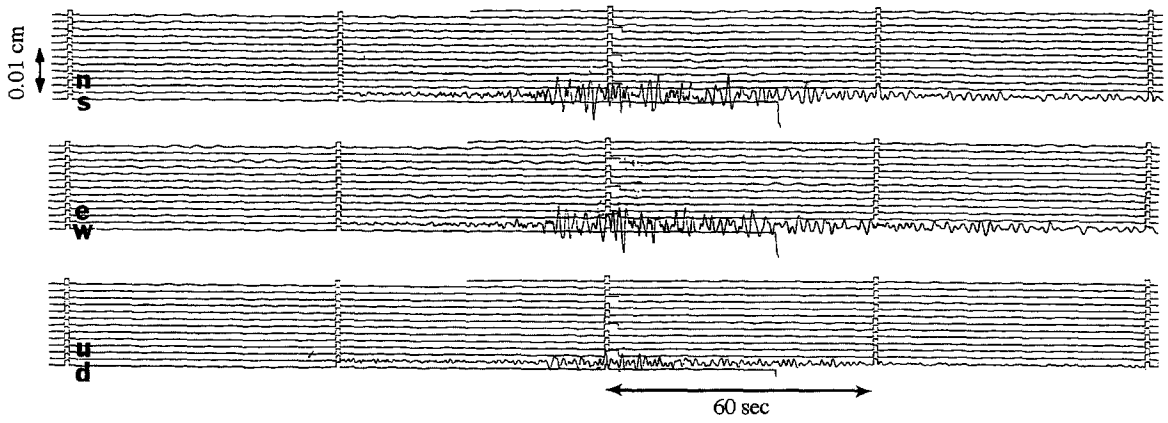

Figure 13. The seismogram recorded by the JMA-59 type seismograph at station SND (R = 375 km).

phase from the top of the lowermost crust with an S-wave velocity of 3.9 km/sec. These phases are labeled Sm-1S and sSm-1S respectively in the synthetic seismograms in Figure 8. Figure 9 shows the theoretical dispersion curves of the fundamental-mode Love and Rayleigh waves for the preferred model LS. Figure 10 compares the observed dispersion characteristics on the transverse and vertical components using a multiple-filter technique with the theoretical group delay times of the fundamental-mode Love and Rayleigh waves, respectively. It is found that the fundamental mode is the dominant arrival for periods greater than 6 sec for both Love and Rayleigh waves.

Waveform Modeling at Station GIF

Figure 11 shows a copy of the original three-component displacement seismograms at station GIF recorded by the JMA-59 type seismograph from the 1990 Odarawa earthquake. We digitized these records at a rate of 10 samples/sec and carefully removed the distortion of the original records due to the mechanism of the recording system, including the instrument pen arc and the instrument response. Then we compared the data with the f-k synthetic seismograms calculated using the preferred velocity model LS, which is constructed for station INU. In the comparison, both the data and the synthetics were bandpass filtered in the following manner. We fixed the cutoff frequency of the high-pass filter at 0.067 Hz considering the noise level, while we changed the cutoff frequency of the low-pass filter in order to identify the frequency range that is not affected by the local site conditions around station GIF. Figure 12 compares the three-component (N–S, E–W, and UD) waveform data (top traces) with the synthetic seismograms with a cutoff frequency of 0.33 Hz for the low-pass filter (second traces). They are in good agreement in terms of travel times, amplitudes, and waveforms for the main part of the seismograms. This result reveals that the preferred velocity model LS established at station INU can be used for simulation of the seismograms recorded at station GIF from the 1923 Kanto earthquake at periods greater than 3 sec and that broadband data are very effective for constructing a crustal structure model if a broadband station exists near the target station.

Waveform Modeling at Station SND

A seismogram from the 1923 Kanto earthquake was also recorded at the Mukaiyama observatory of Tohoku University in Sendai, which is located about 350 km north of the epicenter (Shiratori, 1924; Kudo, 1981; Kataoka and Sato; 1994; Takemura *et al.*, 1995). Since this observatory was closed in 1931, seismograms from modern events are

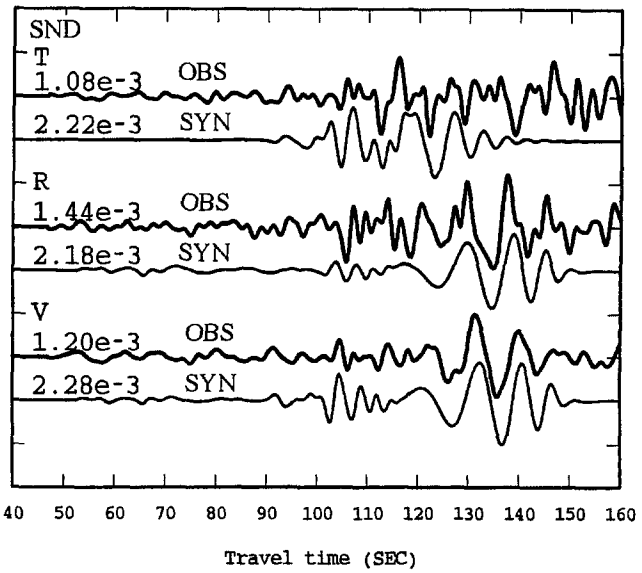

Figure 14. Comparison between the three-component, whole waveform data (upper traces) and the synthetic waveforms (lower traces) for the velocity model given in Table 8 at station SND (R = 375 km). A bandpass filter from 0.067 to 0.33 Hz is applied to both the data and synthetics. The numbers above the traces are the absolute peak amplitudes in 10^{-3} cm. The origin time is assumed to be 7:13:01.69 sec (GT).

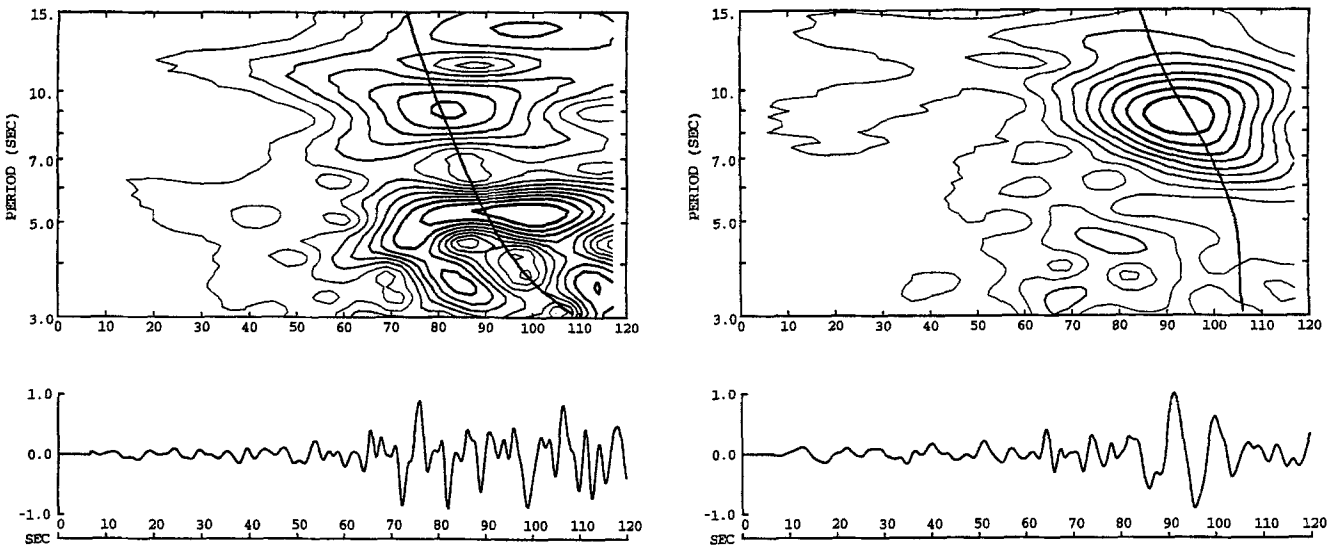

(a) Transverse component (b) Vertical component

Figure 15. (a) Dispersion characteristics of the observed transverse-component displacement motion at station SND (R = 375 km). The nonstationary spectrum is calculated by the multiple-filter technique. The solid line denotes the group delay time of the fundamental-mode Love wave for the velocity model given in Table 8. The origin time is assumed to be 7:13:01.69 sec (GT). (b) Dispersion characteristics of the observed vertical-component displacement motion at station SND. The solid line denotes the group delay time of the fundamental-mode Rayleigh wave for the velocity model given in Table 8.

not available from the same station. However, seismograms recorded at the JMA Sendai (SND) station, which is located about 4 km northeast of the Mukaiyama observatory, are available for modern events (Table 6). Figure 13 shows a copy of the original three-component displacement seismograms recorded by the JMA-59 type seismograph at SND from the 1990 Odarawa earthquake. Although the quality of the data is not high, we digitized this record considering the importance of propagation path effects for modeling the recorded ground motions from the 1923 Kanto earthquake. The digitization procedure is the same as that used in the data recorded at station GIF. We rotated the horizontal (N–S and E–W) displacement data into the transverse and radial components, and bandpass filtered between 0.067 and 0.33 Hz considering the noise level and local site effects.

Table 8
Velocity Structure Model for Local Station SND

Depth* (km)	Thickness (km)	Vp (km/sec)	Vs (km/sec)	ρ (g/cc)	Qp	Qs
0.0	1.0	3.80	2.00	2.4	200	100
1.0	6.0	5.50	3.24	2.6	300	150
7.0	8.0	6.20	3.64	2.7	300	150
15.0	19.0	6.90	3.94	2.9	500	250
34.0	—	7.80	4.43	3.2	1000	500

*Depth to the top of the layer.

Based on recent tomographic images of the deep velocity structure derived by Zhao *et al.* (1992a, 1992b, 1994) and the Vp/Vs ratios derived by Ukawa and Fukao (1981), we constructed a flat-layered model along the travel path. Since there is no reliable information on the uppermost crust, we determined it by comparing the travel times and waveforms of observed surface waves with those of f-k synthetic seismograms. Figure 14 displays the results of the surface-waveform modeling, in which the NIED origin time is used. The synthetic waveforms from the preferred velocity model listed in Table 8 are in reasonable agreement with the data. The deviation of the amplitudes is within a factor of about 2. In Figure 9, the theoretical dispersion curves of the fundamental-mode Love and Rayleigh waves for the model for SND are displayed with those for station GIF. Regionalized velocity models are needed (e.g., Thio and Kanamori, 1995) since there are differences in dispersion characteristics from path to path. Figure 15 compares the observed dispersion characteristics of the transverse and vertical components using a multiple-filter technique with the theoretical group delay times of the fundamental-mode Love and Rayleigh waves, respectively. A good fit is obtained at periods greater than 6 to 7 sec. We believe that it is appropriate to use this preferred velocity model when we simulate the seismogram of the 1923 Kanto earthquake recorded at Mukaiyama observatory in our companion article (Sato *et al.*, 1998).

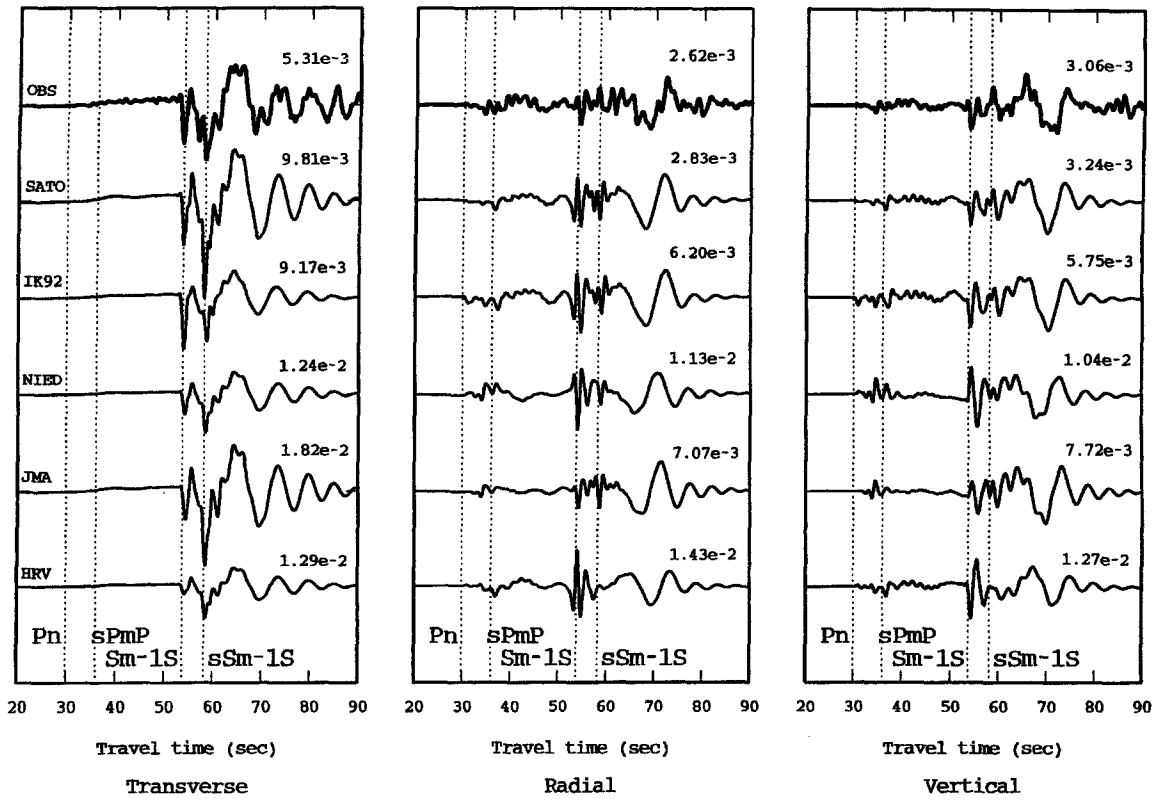

Figure 16. Comparison between displacement waveform data and synthetic waveforms for various focal mechanisms given in Table 1 at station INU (R = 190 km). Both the data and synthetics are bandpass filtered between 0.02 and 1.00 Hz. The synthetic seismograms with various focal mechanisms are calculated with the corresponding depth and seismic moment given in Table 1. The amplitude of each trace is normalized by the maximum amplitude of the corresponding radial component in order to facilitate comparison of the amplitude ratios between three components. The absolute maximum amplitudes are indicated on the right of each trace in 10^{-3} cm. The origin time is assumed to be 7:13:01.69 sec (GT). The phases *Sm-1S* and *sSm-1S* are identified.

Discussion and Conclusions

Effect of Source Mechanism on Waveform Modeling

We used the Odawara earthquake of 5 August 1990 (M 5.1), which is the first magnitude 5 earthquake in the past 60 years near the hypocenter of the 1923 Kanto earthquake (Ms 8.2), as a path-calibration event. The source parameters that we obtained for this event (a source depth of 15.3 km, a dip of 35°, a rake of 40°, a strike of 215°, a seismic moment of 3.3 $\times$ 10^{23} dyne-cm, a source duration of 0.65 sec, and a stress drop of 170 bars) are different from those of the previous solutions.

The contribution of the source mechanism on local seismograms is quite significant as Pitarka *et al.* (1994) pointed out. For example, at station HNG, the transverse-component synthetic waveforms for dip-slip type mechanisms (the IK92 and HRV CMT solutions) are much different from those for the other mechanisms and the data as shown in Figure 5d. If we use these solutions in estimating velocity models without re-estimating the source mechanism, we may obtain incorrect velocity models.

The source mechanism affects regional seismograms as well. Figure 16 compares synthetic waveforms for the various source mechanisms at station INU. The relative strengths of the phases *Sm-1S* and *sSm-1S* with the dip-slip type mechanisms (the IK92 and HRV CMT solutions) are different from those of the data. Although strike-slip mechanisms (the NIED and JMA solutions) reproduce the relative strengths of the *SH* pulses on the transverse component, they do not provide a good explanation of the observed *Pnl* phases on the radial and vertical components. Moreover, for the various source models, there are apparent differences in the arrival times of the wave packet that includes Rayleigh waves. In particular, this wave packet for the NIED solution arrives about 3 to 4 sec earlier than those for the data and the other mechanisms. If we had used the NIED solution (which was judged to be the most appropriate solution by Pitarka *et al.*, 1994) in our surface-waveform modeling, we would have obtained a velocity structure model with slower-velocity uppermost layers. This demonstrates that path corrections require a well-calibrated source model.

Table 9
Velocity Structure Models in the Southern Kanto District

Model	Depth* (km)	Thickness (km)	*Vp* (km/sec)	*Vs* (km/sec)	*ρ* (g/cc)	*Qp*	*Qs*
L4†	0.0	2.7	2.80	1.30	2.3	200	100
	2.7	3.4	5.60	2.90	2.5	400	200
	6.1	12.9	6.00	3.40	2.6	500	230
	19.0	—	6.80	4.00	3.0	600	270
L5†	0.0	1.0	1.83	0.70	2.0	100	50
	1.0	1.7	2.80	1.30	2.3	200	100
	2.7	3.4	5.60	2.90	2.5	400	200
	6.1	12.9	6.00	3.40	2.6	500	230
	19.0	—	6.80	4.00	3.0	600	270
Y1‡	0.0	1.1	1.83	0.60	1.8	60	30
	1.1	0.9	3.24	1.19	2.2	150	75
	2.0	2.1	4.76	2.53	2.4	300	150
	4.1	7.9	5.60	2.90	2.5	300	150
	12.0	12.0	6.15	3.40	2.7	300	150
	24.0	10.0	6.70	3.70	2.9	500	250
	34.0	—	7.50	4.30	3.2	1000	500
Y2‡	0.0	0.5	1.70	0.50	1.5	60	30
	0.5	0.6	2.10	0.80	1.9	100	50
	1.1	0.9	3.24	1.19	2.2	150	75
	2.0	0.8	4.76	2.53	2.4	300	150
	2.8	10.0	5.60	3.30	2.5	300	150
	12.8	13.0	6.15	3.60	2.7	300	150
	25.8	10.0	6.70	3.70	2.9	500	250
	35.8	—	7.50	4.30	3.2	1000	500

*Depth to the top of the layer.

†Models L4 and L5 are the same as those used in Takeo and Kanamori (1992).

‡Models Y1 and Y2 are the same as the models 1 and 2 used in Yamazaki *et al.* (1992), except the *Qp* and *Qs* are our assumed values.

Comparison of Various Flat-Layered Models in the Southern Kanto District

The preferred velocity model for station HNG obtained in this study is used in the simulation of the seismograms of the 1923 Kanto earthquake recorded at station HNG in our companion article (Sato *et al.*, 1998). In the southern Kanto district, several flat-layered models have been developed in previous studies. Here we investigate the sensitivity of these velocity models to synthetic waveforms at HNG.

Takeo and Kanamori (1992) used two velocity models L4 and L5 (Table 9) in the simulation of long-period ground motions at HNG from the 1923 Kanto earthquake. Model L4 was derived from the results of an explosion experiment that revealed the depth of bedrock beneath Tokyo (Research Group on Underground Structure in Tokyo, 1989) in conjunction with the velocity structure in Sagami Bay used in Yamanaka (1991). The model L5 introduces a soft sedimentary layer with an *S*-wave velocity of 0.7 km/sec in model L4.

Yamazaki *et al.* (1992) developed two velocity structure models Y1 and Y2 given in Table 9 from the observed dispersion characteristics of surface waves in the Kanto Plain. Model Y2 is characterized by its thinner sedimentary layers above bedrock than model Y1. Yamazaki *et al.* (1992) showed that model Y1 is applicable as an average velocity structure between HNG and the Koto area in the central part of the Kanto plain, while model Y2 can be used as an average velocity structure for the western part of the Kanto plain including station ASK. Kinoshita *et al.* (1992) showed that the dispersion characteristics from model Y1 are consistent with the results from the array observation of surface waves in the Koto area.

Figure 17 compares the recorded waveforms of the 1990 Odawara earthquake with synthetic seismograms using various structure models at station HNG. These waveforms are bandpass filtered between 0.10 and 0.33 Hz. The waveforms from the preferred model obtained in this study show the best agreement with the data. Models L5 and Y1 cannot reproduce the data well, while models L4 and Y2 work fairly well. This result reveals the importance of modeling the sedimentary layers shallower than a few kilometers.

Comparison of the Preferred Velocity Model with the Previous Velocity Model for Station GIF

Using Love waves generated by the 1974 Izu-Hanto-Oki earthquake (M_{JMA} 6.9) and the 1980 Izu-Hanto-Toho-Oki earthquake (M_{JMA} 6.7) (see Fig. 1), Nozawa *et al.* (1996) recently estimated a flat-layered model (LK) along the central and southern Izu Peninsula to station GIF (Table 10). The third traces in Figure 12 represent waveforms calculated using the LK model at GIF. The synthetic surface waves for the LK model are delayed with respect to both the data and the synthetic seismograms for the preferred model obtained in this study. In particular, the synthetic Love waves calculated using the LK model are delayed about half of a wavelength compared with the data. One of the reasons may be that since the travel path along the central and southern Izu Peninsula to station GIF is across Suruga Bay, the waveforms are affected by slower velocity layers in Suruga Bay (Hasegawa *et al.*, 1989). We believe that the 1990 Odawara earthquake is more suitable as a calibration event for the 1923 great Kanto earthquake than the Izu earthquakes since the hypocenter of the 1990 Odawara earthquake is much closer to the hypocenter and the locations of large asperities of the

Table 10
Velocity Structure Model between the Izu Peninsula and GIF Station

Model	Depth* (km)	Thickness (km)	*Vp* (km/sec)	*Vs* (km/sec)	*ρ* (g/cc)	*Qp*	*Qs*
LK†	0.0	2.5	3.90	2.20	2.5	200	100
	2.5	1.0	5.10	2.70	2.6	300	150
	3.5	12.5	6.00	3.50	2.7	300	150
	16.0	16.0	6.80	3.80	2.9	500	250
	32.0	—	7.60	4.25	3.1	1000	500

*Depth to the top of the layer.

†This model is the same as that used in Nozawa *et al.* (1995), except the *Qp* and *Qs* values are our assumed values.

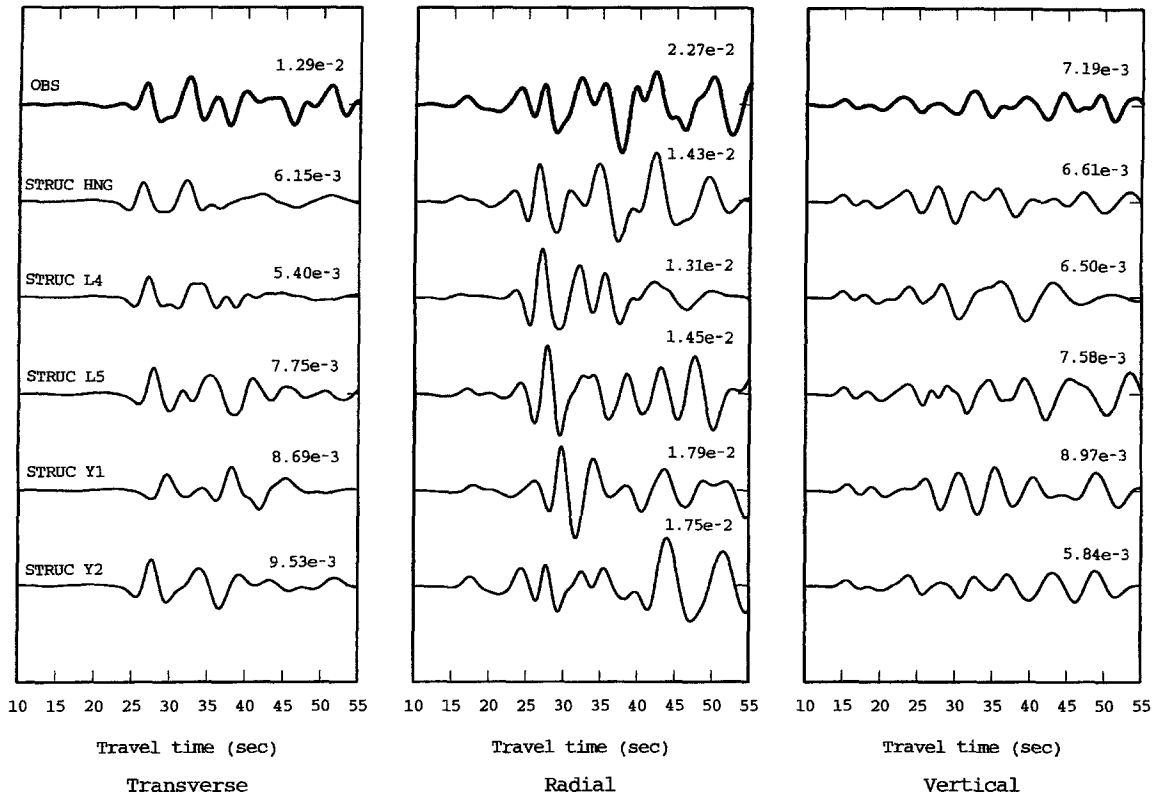

Figure 17. Comparison between the three-component, whole waveform data (top traces) of the HNG recording of the 1990 Odawara earthquake with synthetic waveforms (second through bottom traces) for various velocity models given in Tables 4 and 9 at station HNG (R = 82.0 km). The second traces are for the velocity model used in this study (in Table 4); the third ones are for model L4; the fourth ones are for model L5; the fifth ones are for model Y1; the bottom ones are for model Y2. A bandpass filter from 0.067 to 0.33 Hz is applied to both the data and synthetics. The numbers on the right of each trace are the absolute peak amplitudes in 10^{-3} cm. The origin time is assumed to be 7:13:01.69 sec (GT).

1923 Kanto earthquake (Wald and Somerville, 1995) than those of the Izu earthquakes.

We believe that the path-specific flat-layered velocity models for stations HNG, GIF, and SND (Tables 4, 7, and 8) developed in this study can be used to simulate seismograms including direct surface waves at periods greater than about 3 sec, which were recorded at these stations from the 1923 Kanto earthquake in the companion article (Sato *et al.*, 1998).

Acknowledgments

This study was done while one of the authors (T.S.) was a visiting associate at the Seismological Laboratory, California Institute of Technology on leave from Izumi Research Institute, Shimizu Corporation. We would like to express our gratitude to Mr. S. Kataoka (Shimizu Corporation) for informative interactions through the period of this project. We would like to thank Drs. K. Kudo (Earthquake Research Institute, the University of Tokyo), S. Zama (Fire Research Institute, Ministry of Home Affairs), and K. Seo and T. Samano (Tokyo Institute of Technology) for providing us with the strong-motion data. We would like to thank Drs. K. Yamaoka and K. Ishihara (Nagoya University) for providing us with the STS-1 broadband data. We are grateful to Drs. F. Kusano and H. Suzuki and other staff members of the Japan Meteorological Agency for providing us with copies of the original recordings of the strong-motion data. We would like to thank to Dr. S. Hori (National Research Institute for Earth Science and Disaster Prevention) for providing us with the information on the source mechanism. We are especially grateful to Dr. M. Takemura (Kajima Corporation) for providing us with his articles on the 1923 Kanto earthquake. We are also grateful to Drs. H. Kanamori (California Institute of Technology), M. Kikuchi (Yokohama City University), M. Ishida (National Research Institute for Earth Science and Disaster Prevention), D. Wald (U.S. Geological Survey), D. Zhao (Washington University), X. Song (California Institute of Technology), and A. Pitarka (Kyoto University) for valuable discussions. Finally, we thank Drs. Arthur F. McGarr and John E. Vidale and an anonymous reviewer for their comments that helped improve the manuscript.

References

Ando, M. (1971). A fault-origin model of the Great Kanto earthquake of 1923 as deduced from geodetic data, *Bull. Earthquake Res. Inst. Tokyo Univ.* **49,** 19–32.

Ando, M. (1974). Seismo-tectonics of the 1923 Kanto earthquake, *J. Phys. Earth* **22,** 263–277.

Asano, S., Y. Yasui, K. Hirama, K. Wakamatsu, T. Kuwahara, S. Okuda, H. Suzuki, K. Kasahara, F. Yamamizu, T. Ikawa, and Y. Ohta (1991).

Seismic reflection profiling in the Tokyo metropolitan area, 2. Velocity an attenuation of seismic waves as derived from VSP in Fuchu, Tokyo metropolis (abstracts), *Seismol. Soc. Japan,* no. 2, 150 (in Japanese).

Ashiya, K., S. Asano, T. Yoshii, M. Ishida, and T. Nishiki (1987). Simultaneous determination of the three-dimensional crustal structure and hypocenters beneath the Kanto-Tokai District, Japan, *Tectonophysics* **140,** 12–27.

Brune, J. N. (1970). Tectonic stress and the spectra of seismic shear waves from earthquakes, *J. Geophys. Res.* **75,** 4997–5009.

Brune, J. N. (1971). Correction, *J. Geophys. Res.* **76,** 5002.

Dreger, D. S. and D. V. Helmberger (1991). Source parameters of the Sierra Madre Earthquake from regional and local body waves, *Geophys. Res. Lett.* **18,** 2015–2018.

Dreger, D. S. and D. V. Helmberger (1993). Determination of source parameters at regional distances with three-component sparse network data, *J. Geophys. Res.* **98,** 8107–8215.

Dziewonski, A., S. Bloch, and M. Landisman (1969). A technique for the analysis of transient seismic signals, *Bull. Seism. Soc. Am.* **59,** 427–444.

Dziewonski, A. M., G. Ektrom, J. H. Woodhouse, and G. Zwart (1991). Centroid-moment tensor solutions for July–September, 1990, *Phys. Earth Planet. Interiors* **67,** 211–220.

Fan, G. and T. Wallance (1991). The determination of source parameters for a small earthquakes from a single, very broadband seismic station, *Geophys. Res. Lett.* **18,** 1385–1388.

Geotechnical Survey Subcommittee on the Ashigara Valley Blind Prediction Test, the Japanese Working Group on Seismic Motion (prepared by K. Kudo) (1992). Geotechnical data, in *Proc. of International Symposium on Effects of Surface Geology on Seismic Motion,* 29–42.

Graves, R. W. (1993). Modeling three-dimensional site response effects in the Marina district basin, San Francisco, California, *Bull. Seism. Soc. Am.* **83,** 1042–1063.

Hamada, N. (1987). Note on the focal depth of the 1923 Great Kanto Earthquake, *Quarterly J. Seismol., Japan Meteorol. Agency* **50,** 1–6 (in Japanese).

Hasegawa, I., K. Ito, M. Takahashi, and S. Iizuka (1989). Velocity structure profile as derived from seismic observations of Kamiyasaku-Izu Oshima explosions (abstracts), *Seismol. Soc. Japan,* no. 2, 202 (in Japanese).

Helmberger, D. V. (1983). Theory and application of synthetic seismograms, in Earthquakes: Observation, Theory, and Interpretation, *Proc. Int. Sch. Phys. 'Enrico Fermi' Course LXXXV,* H. Kanamori and E. Boschi (Editors), North-Holland, Amsterdam, 174–221.

Helmberger, D. V. and G. R. Engen (1980). Modeling the long-period body waves from shallow earthquakes at regional ranges, *Bull. Seism. Soc. Am.* **70,** 1699–1714.

Helmberger, D. V., P. G. Somerville, and E. Garnero (1992a). The location and source parameters of the Lompoc, California, Earthquake of 4 November 1927, *Bull. Seism. Soc. Am.* **82,** 1678–1709.

Helmberger, D. V., R. Stead, P. Ho-Liu, and D. Dreger (1992b). Broadband modelling of regional seismograms: Imperial Valley to Pasadena, *Geophys. J. Int.* **110,** 42–54.

Helmberger, D. V., D. Dreger, R. Stead, and H. Kanamori (1993). Impact of broadband seismology on the understanding of strong motions, *Bull. Seism. Soc. Am.* **83,** 830–850.

Higashi, S. (1994). Strong-motion characteristics considering two- and three-dimensional effects of velocity structures—Quantitative estimation based on observational and theoretical studies, *Ph.D. Thesis,* University of Tokyo, Tokyo (in Japanese).

Higashi, S. and K. Kudo (1992). Polarization and frequency-wavenumber spectrum analysis for the strong-motion array data in the Ashigara Valley, Japan, *J. Phys. Earth* **40,** 5–25.

Hisada, Y. Aki, and T. L. Teng (1993). 3-D simulations of surface wave propagation in the Kanto sedimentary basin, Part 2: Application of the surface wave BEM, *Bull. Seism. Soc. Am.* **83,** 1700–1720.

Ikami, A. (1978). Crustal structure in the Shizuoka district, central Japan as derived from explosion seismic observations, *J. Phys. Earth* **26,** 299–331.

Ishida, M. and A. Hasemi (1990). The three-dimensional P- and S-wave velocity structure in the Kanto-Tokai district, Japan, Abstracts, Joint Meeting of Japan Earth and Planetary Science, 95 (in Japanese).

Ishida, M. and M. Kikuchi (1992). A possible foreshock of a future large earthquake near Odawara, central Japan, *Geophys. Res. Lett.* **19,** 1695–1698.

Japan Meteorological Agency (1990). On the earthquake (M 5.1) in the Western Part of Kanagawa Prefecture, August 5, 1990, *Rep. Coordinating Committee Earthquake Prediction* **45,** 206–212 (in Japanese).

Kakimi, T. (1973). Neotectonic Map Tokyo, Geological Survey of Japan.

Kakishita, T., I. Sasakawa, M. Kobayashi, A. Nagai, and N. Hamada (1992). An examination of JMA formulas for determining magnitude using data obtained by the JMA-87 type electromagnetic strong motion seismograph, *Zishin (J. Seismol. Soc. Japan)* **45,** 263–277.

Kanamori, H. (1971). Faulting of the great Kanto earthquake of 1923 as revealed by seismological data, *Bull. Earthquake Res. Inst. Tokyo Univ.* **49,** 13–18.

Kanamori, H. (1974). Long-period ground motion in the epicentral area of major earthquakes, *Tectonophysics* **21,** 341–356.

Kanamori, H. and S. Miyamura (1970). Seismological re-evaluation of the great Kanto earthquake of September 1, 1923, *Bull. Earthquake Res. Inst. Tokyo Univ.* **48,** 115–125.

Kataoka, S. and T. Sato (1994). Relationship between peculiar phases in seismograms observed at regional sites, Tokushima and Sendai and asperities for the 1923 Kanto earthquake, *Proc. of the 9th Symposium Japanese Earthquake Engineering,* Vol. 1, 583–588 (in Japanese).

Kataoka, S., T. Sato, and I. Muramatsu (1995). Digitization and processing for the 1923 Kanto earthquake seismograms obtained at Tokushima JMA observatory, *Zishin (J. Seismol. Soc. Japan)* **48,** 235–246 (in Japanese).

Kato, K., K. Aki, and T. L. Teng (1993). 3-D simulations of surface wave propagation in the Kanto sedimentary basin, Part 1: Application of the surface wave Gaussian beam method, *Bull. Seism. Soc. Am.* **83,** 1676–1699.

Kawai, K. (1965). Natural gas geology of the southern Kanto region, Japan. Agenda Item 6. Contribution from the Government of Japan to ECAFE 3rd Petroleum Symposium, 1–18.

Kikuchi, M. and Y. Fukao (1987). Inversion of long-period P waves from great earthquakes along subduction zones, *Tectonophysics* **144,** 231–247.

Kinoshita, S., H. Fujiwara, T. Mikoshiba, and T. Hishino (1992). Secondary Love waves observed by a strong-motion array in the Tokyo lowlands, Japan, *J. Phys. Earth* **40,** 99–116.

Koketsu, K. and S. Higashi (1992). Three-dimensional topography of the sediment/basement interface in the Tokyo metropolitan area, central Japan, *Bull. Seism. Soc. Am.* **82,** 2328–2349.

Kudo, K. (1980). The contribution of Love waves to strong ground motions, *Proc. of the 7th World Conf. Earthquake Engineering,* Vol. 2, 499–506.

Kudo, K. (1981). Ground motion at Hongo in Tokyo during the 1923 great Kanto earthquake based on seismograms observed at the Mukaiyama observatory of Tohoku Imperial University at Sendai (abstracts), *Seismol. Soc. Japan,* no. 1, 232 (in Japanese).

Kudo, K., E. Shima, and M. Sakaue (1988). Digital strong motion accelerograph array in Ashigara Valley—Seismological and engineering prospects of strong motion observation, *Proc. of the 9th World Conf. Earthquake Engineering,* Vol. 2, 289–296.

Lees, J. M. and M. Ukawa (1992). The South Fossa Magna, Japan, revealed by high-resolution P- and S-wave travel time tomography, *Tectonophysics* **207,** 377–396.

Liu, H. and T. Heaton (1984). Array analysis of the ground velocities and accelerations from the 1971 San Fernando, California, earthquake, *Bull. Seism. Soc. Am.* **74,** 1951–1968.

Masaki, K. and K. Iida (1981). On the ground structure of Nagoya area. I, Observations of seismic waves generated from the 1st Nagoya-Nabeta explosion, *Bull. AICHI Inst. Technol.* **16,** 165–173.

Masaki, K. and K. Iida (1982). On the ground structure of Nagoya area. II, Observations of seismic waves generated from the 2nd Nagoya-Nabeta and 1st Toyohashi-Tahara explosion, *Bull. AICHI Inst. Technol.* **17,** 159–171.

Matsu'ura, M., T. Iwasaki, Y. Suzuki, and Y. Sato (1980). Statical and dynamical study on faulting mechanism of the 1923 Kanto earthquake, *J. Phys. Earth* **28,** 119–143.

Matsu'ura, R. S., T. Yoshii, T. Moriya, H. Miyamachi, Y. Sasaki, A. Ikami, and M. Ishida (1991). Crustal structure of a seismic-refraction profile across the Median and Akaishi tectonic lines, central Japan, *Bull. Earthquake Res. Inst. Tokyo Univ.* **66,** 497–516.

Minashi, S., N. Nasu, H. Nirei *et al.* (1979). Geological map in and around the Tokyo Bay, Geological Survey of Japan.

Miyakoshi, K., H. Okada, T. Sasatani, T. Moriya, S. Ling, and S. Saito (1994). Estimation of geological structure under ESG blind prediction test sites in Odawara City by using microtremors, *Zishin (J. Seismol. Soc. Japan)* **47,** 273–285.

Morioka, T. (1980). The ground motion of the great Kwanto earthquake of 1923, *Trans. Architectural Inst. Japan* **289,** 79–88.

Morioka, T. and M. Yamada (1986). An attempt to estimate the maximum ground motion of the great Kanto earthquake of 1923, *Proc. of the 7th Symposium Japanese Earthquake Engineering,* 109–114 (in Japanese).

Muramatsu, I. (1977). A velocity type strong motion seismograph with wide frequency range, *Zishin (J. Seismol. Soc. Japan)* **30,** 317–338 (in Japanese).

Nasu, N. (1971a). Extremely strong ground motion 1, *Architectural Eng.,* no. 4, 123–127 (in Japanese).

Nasu, N. (1971b). Extremely strong ground motion 2, *Architectural Eng.,* no. 5, 123–127 (in Japanese).

National Research Institute for Earth Science and Disaster Prevention (1990). The earthquake in the Western Part of Kanagawa Prefecture (August 5, 1990), *Rep. Coordinating Committee Earthquake Prediction* **45,** 213–220 (in Japanese).

Nishizawa, A., T. Kanazawa, T. Iwasaki, and H. Shimamura (1996). Crustal structure related to the Philippine Sea plate subduction in the northeastern part of the Sagami Trough, Japan, *Phys. Earth Planet. Sci.* **93,** 21–36.

Nozawa, T., M. Takemura, H. Yamanaka, and T. Ikeura (1996). Source characteristics of the 1923 Kanto earthquake inferred from long-period strong motion data, Part. 1 Simulation of seismograms at the Gifu station, *Zishin (J. Seismol. Soc. Japan)* **48,** 331–340 (in Japanese).

Pitarka, A. S., H. Takenaka, and D. Suetsugu (1994). Modeling strong motion in the Ashigara Valley for the 1990 Odawara, Japan, earthquake, *Bull. Seism. Soc. Am.* **84,** 1327–1335.

Research Group on Underground Structure in the Tokyo Metropolitan Area (1989). Technical report on the Yumenoshima seismic refraction experiment (in Japanese).

Saikia, C. K. (1994). Modified frequency-wavenumber algorithm for regional seismograms using Filon's quadrature: modelling of Lg waves in eastern North America, *Geophys. J. Int.* **118,** 142–158.

Saikia, C. K. and R. B. Herrmann (1987). Determination of focal mechanism solutions for four earthquakes from Monticello, South Carolina, and crustal structure by waveform modelling, *Geophy. J. R. Astr. Soc.* **90,** 669–691.

Samano, T. and K. Seo (1988). Influence of deep underground structure characteristics of rather long-period ground motions, *Proc. of the 9th World Conf. Earthquake Engineering,* Vol. 2, 591–596.

Sasaki, Y., K. Nakamura, and N. Furuhashi (1984). Velocity structure in the northern part of Gifu City (abstracts), *Seismol. Soc. Japan,* no. 2, 229 (in Japanese).

Sasatani, T., T. Yoshii, A. Ikami, T. Tanada, T. Nishiki, and S. Kato (1990). Upper crustal structure under the central part of Japan: Miyata-Shikishima profile, *Bull. Earthquake Res. Inst. Tokyo Univ.* **65,** 33–48.

Sato, R. (1979). Theoretical basis on relationships between focal parameters and earthquake magnitude, *J. Phys. Earth* **27,** 353–372.

Sato, T., R. W. Graves, P. G. Somerville, and S. Kataoka (1998). Estimates of regional and local strong motions during the great 1923 Kanto, Japan earthquake (Ms 8.2), Part 2: Forward simulation of seismograms using variable-slip rupture models and estimation of near-fault long-period ground motions, *Bull. Seism. Soc. Am.* **88,** 206–227.

Shiratori, K. (1924). Notes on the destructive earthquake in Sagami Bay on the first of September, 1923, *Japan J. Astr. Geophys.* **2,** 173–192.

Subcommittee of the Earthquake Data Selection, the Japanese Working Group on the Effects of Surface Geology on Seismic Motion (prepared by K. Kudo) (1992). Earthquake motions: given and blinded data, *Proc. International Symposium on Effects of Surface Geology on Seismic Motion,* 53–60.

Suzuki, H. (1993). Basal structure of the northern Tokyo Bay area—Logging data of the Koto observation well (abstracts), *Japan Earth Planet. Sci. Joint Meeting,* 214 (in Japanese).

Suzuki, H. (1995). Shear wave velocity structure of the metropolitan area (abstracts), *Japan Earth Planet. Sci. Joint Meeting,* 594 (in Japanese).

Takemura, M. (1994). Aftershock activities for two days after the 1923 Kanto earthquake (M = 7.9) inferred from seismograms at Gifu observatory, *Zishin (J. Seismol. Soc. Japan)* **46,** 439–455 (in Japanese).

Takemura, M. and N. Hamada (1994). Characteristics of P-waves from the 1923 Kanto Earthquake observed at Meteorological observatories in and around Japan (abstracts), *Seismol. Soc. Japan,* no. 1, 122 (in Japanese).

Takemura, M. and T. Nozawa (1994). Strong motion seismograms for the 1923 Kanto Earthquake and its aftershocks at Takada Meteorological Observatory (abstracts), *Seismol. Soc. Japan,* no. 1, 226 (in Japanese).

Takemura, M., T. Ikeura, K. Kudo, and H. Ohnuma (1994). Strong motion records from the 1923 Kanto earthquake observed at the Gifu observatory, *Zishin (J. Seismol. Soc. Japan)* **47,** 193–200 (in Japanese).

Takemura, M., K. Kudo, T. Nozawa, T. Sato, and S. Kataoka (1995). Strong motion records from the 1923 Kanto earthquake observed at the Mukaiyama observatory of Tohoku Imperial University at Sendai, *Zishin (J. Seismol. Soc. Japan)* **48,** 297–306 (in Japanese).

Takeo, M. and H. Kanamori (1992). Simulation of long-period ground motions for the 1923 Kanto earthquake (M = 8), *Bull. Earthquake Res. Inst. Tokyo Univ.* **67,** 389–436.

Tanaka, T., S. Yoshizawa, T. Morishita, K. Osada, and Y. Osawa (1973). Observation and analysis of underground earthquake motion, *Proc. of the 5th World Conference Earthquake Eng.,* Vol. 1, 658–667.

Thio, H. K. and H. Kanamori (1995). Moment tensor inversions for local earthquakes using surface waves recorded at TERRAscope, *Bull. Seism. Soc. Am.* **85,** 1021–1038.

Toshinawa, T. and T. Ohmachi (1992). Love-wave propagation in a three-dimensional sedimentary basin, *Bull. Seism. Soc. Am.* **82,** 1661–1677.

Ukawa, M. and Y. Fukao (1981). Poisson's ratio of the upper and lower crust and the sub-moho mantle beneath central Honshu, Japan, *Tectonophysics* **77,** 233–256.

Vidale, J. E. and D. V. Helmberger (1988). Elastic finite-difference modeling of the 1971 San Fernando, California, Earthquake, *Bull. Seism. Soc. Am.* **78,** 122–141.

Wald, D. J. and P. G. Somerville (1995). Variable-slip rupture model of the great 1923 Kanto, Japan, Earthquake: geodetic and body-waveform analysis, *Bull. Seism. Soc. Am.* **85,** 159–177.

Wald, D. J., H. Kanamori, D. V. Helmberger, and T. H. Heaton (1993). Source study of the 1906 San Francisco Earthquake, *Bull. Seism. Soc. Am.* **83,** 981–1019.

Walter, W. R. (1993). Source parameters of the June 29, 1992 Little Skull Mountain Earthquake from complete regional waveforms at a single station, *Geophys. Res. Lett.* **20,** 403–406.

Yamada, I., Y. Fukao, Y. Ishihara, and H. Aoki (1989). Broad-band and wide dynamic range seismic observation by an STS-seismograph, *Zishin (J. Seismol. Soc. Japan),* 21–31 (in Japanese).

Yamamizu, F., H. Takahashi, N. Goto, and Y. Ohta (1981). Shear wave

velocities in deep soil deposits (Part 3), *Zishin (J. Seismol. Soc. Japan)* **34,** 465–479 (in Japanese).

Yamamizu, F., K. Kasahara, H. Suzuki, I. Adachi, Y. Ohta, and T. Ikawa (1995). Seismic reflection profiling around the Kohto deep well (1) (abstracts), *Seismol. Soc. Japan,* no. 2, 636 (in Japanese).

Yamanaka, H. (1991). Analysis and modeling of long-period ground motion in the Kanto plain, Japan, *Proc. of the 4th International Conference Seismic Zonation,* 75–82.

Yamanaka, H., K. Seo, and T. Samano (1989). Effects of sedimentary layers on surface-wave propagation, *Bull. Seism. Soc. Am.* **79,** 631–644.

Yamanaka, H., K. Seo, and T. Samano (1992). Analysis and numerical modeling of surface-wave propagation in a sedimentary basin, *J. Phys. Earth* **40,** 57–71.

Yamanaka, H., K. Seo, T. Samano, E. Shima, and T. Nozawa (1993). Seismic prospectings in the southwestern part of the Tokyo metropolitan area (5) (abstracts), *Japan Earth Planet. Sci. Joint Meeting,* 213 (in Japanese).

Yamazaki, K., M. Minamishima, and K. Kudo (1992). Propagation characteristics of intermediate-period (1–10 seconds) surface waves in the Kanto Plain, Japan, *J. Phys. Earth* **40,** 117–136.

Yokota, H., S. Kataoka, and T. Tanaka (1989). Estimation of long-period ground motion of the 1923 great Kanto earthquake, *J. Struct. Constr. Eng., Architectural Inst. Japan* **401,** 35–45 (in Japanese).

Yoshii, T., S. Asano, S. Kubota, Y. Sasaki, H. Okada, T. Masuda, T. Moriya, and H. Murakami (1985). Crustal structure in Izu Peninsula, central Japan, as derived from explosion seismic observations, 2. Ito-Matsuzaki profile, *J. Phys. Earth* **33,** 435–451.

Zama, S. (1992). Characteristics of long-period ground motions in Tokyo Bay area, Japan, *Proc. of the 10th World Conference Earthquake Engineering* 593–598.

Zhao, L. S. and D. V. Helmberger (1994). Source estimation from broadband regional seismograms, *Bull. Seism. Soc. Am.* **84,** 91–104.

Zhao, D., A. Hasegawa, and S. Horiuchi (1992a). Tomographic imaging of P and S wave velocity structure beneath northeastern Japan, *J. Geophys. Res.* **97,** 19909–19928.

Zhao, D., S. Horiuchi, and A. Hasegawa (1992b). Seismic velocity structure of the crust beneath the Japan Islands, *Tectonophysics* **212,** 289–301.

Zhao, D., A. Hasegawa, and H. Kanamori (1994). Deep structure of Japan subduction zone as derived from local, regional, and teleseismic events, *J. Geophys. Res.* **99,** 22313–22329.

Izumi Research Institute
Shimizu Corporation
Fukoku-seimei Bldg.
2-2-2 Uchisaiwai-cho, Chiyoda-ku
Tokyo 100-0011, Japan
(T.S.)

Seismological Laboratory 252-21
California Institute of Technology
Pasadena, California 91125
(D.V.H.)

Woodward-Clyde
566 El Dorado Street
Pasadena, California 91101
(P.G.S., R.W.G., C.K.S.)

Manuscript received 25 April 1996.